

001
002
003
004
005
006
007
008
009
010
011
012
013
014
015
016
017
018
019
020
021
022
023
024
025
026
027
028
029
030
031
032
033
034
035
036
037
038
039
040
041
042
043
044
045
046

The Importance of Initial Conditions in Seasonal Predictions of Antarctic Sea Ice

Elio Campitelli^{1,2*}, Ariaan Purich^{1,2}, Julie Arblaster^{1,2},
Eun-Pa Lim³, Matthew C. Wheeler³, Phillip Reid³

¹School of Earth, Atmosphere and Environment, Monash University, Kulin
Nations, Clayton, Victoria, Australia..

²SARC Special Research Initiative for Securing Antarctica's
Environmental Future, Clayton, Kulin Nations, Victoria, Australia.

³Research, Bureau of Meteorology, Australia.

*Corresponding author(s). E-mail(s): elio.campitelli@monash.edu;

Abstract

Accurate Antarctic sea-ice forecasts are crucial for climate monitoring and operational planning, yet they remain challenging due to model biases and complex ice-ocean-atmosphere interactions. The two versions of the Australian Bureau of Meteorology's ACCESS seasonal forecast system, ACCESS-S1 and ACCESS-S2, use identical model configuration and differ only in their initial conditions; primarily in that ACCESS-S2 does not assimilate sea-ice observations, whereas ACCESS-S1 does.

This provides a convenient opportunistic experiment to assess the role of initial conditions on Antarctic sea-ice forecasts using more than 20 years of fully coupled simulations with two 9-member ensembles. Our analysis reveals that both systems experience an extended melt season and delayed growth phase compared with observations. This leads to a significant negative sea-ice extent bias, which is corrected only in ACCESS-S1 by the data assimilation system. The impact of the differing initial conditions on forecast errors varies dramatically by season: summer and autumn initial conditions (January-April) provide predictive skill for up to three months, with February initial conditions being particularly crucial.

047 In contrast, winter forecasts of the two systems are statistically indistinguishable
048 after only two weeks. Regional analysis of forecast skill suggests that this
049 winter predictability barrier is most dramatic over East Antarctica, where even
050 ACCESS-S1 shows negative skill. These findings highlight the critical importance
051 of comprehensive year-round sampling in predictability studies and suggest that
052 operational sea-ice data assimilation efforts should prioritize the summer-autumn
053 period when initial conditions have maximum impact on forecast skill.

054
055 **Keywords:** sea ice, seasonal predictability, initial conditions, forecasting

056
057
058
059

060 **Introduction**

061

062 Accurately modelling Antarctic sea ice is essential for understanding processes and
063 improving climate projections to inform adaptation strategies. Accurate seasonal to
064 sub-seasonal forecasts are also crucial for operation contingency planning in and
065 around the Antarctic continent, including scientific missions, fisheries, and tourism^{1;2}.
066

067 Improvements in modelled sea-ice might also help improve weather forecasts over and
068 away from sea-ice regions^{3–5}.

069

070 However, progress in Antarctic sea-ice forecasting system has lagged behind Arctic
071 sea-ice forecasts due to model biases, and inherent large variability and complexity^{6;7}.
072

073 Dynamical seasonal forecasts of summer Antarctic sea ice have been shown to perform
074 worse than relatively simpler statistical methods⁸ and machine learning approaches (e.g.
075 Dong et al.⁹, Lin et al.¹⁰), which also underscores the need for better understanding
076 and physical modelling of sea-ice dynamics, and drivers of its variability.

077

078 Good initial conditions are generally required for a good forecast, however, it is not
079 entirely known to what extent accurate sea-ice initial conditions affect the quality of
080 the forecast and at what timescales. Exploring seasonal predictions of Arctic sea ice,
081 Guemas et al.¹¹ found that sea-ice initial conditions are important in autumn to predict
082 summer sea ice, but the impact wasn't as dramatic when predicting winter sea ice. Day
083

084

et al.¹² also found seasonally-varying differences in the effect of initialisation, noting that accurate Arctic sea-ice thickness leads to improved sea-ice forecasts initialised in July but not when initialised in January.

For the Antarctic, Holland et al.¹³ studied the initial-value predictability of Antarctic sea ice in a perfect model study using the CCSM3 model. They found that sea-ice and ocean initial conditions provide predictive information to forecast sea-ice edge location several months in advance and that some predictability is retained for up to two years thanks to ocean heat content anomalies that are advected eastward. This is in contrast with Marchi et al.¹⁴, who ran perfect model experiments to argue that uncertainty in the predicted atmospheric state and evolution is the main driver of uncertainty in Antarctic sea-ice extent prediction on seasonal timescales, with sea-ice and ocean initial conditions having lesser importance. More recently, Morioka et al.¹⁵ studied decadal forecasts of Antarctic sea ice and found that initialising ocean and sea ice improved the correlation between simulated and observed sea-ice concentration evolution in the Amundsen–Bellingshausen Sea. It is hard to compare these studies since they are based on forecasts initialised at different times of the year and different frameworks: Holland et al.¹³ ran 20 ensemble members initialised on the 1st of January of a particular year, Marchi et al.¹⁴ ran forecasts from the 1st of March and 1st of September, and Morioka et al.¹⁵ ran forecasts only from the 1st of March. Marchi et al.¹⁴ also used a coupled ocean–sea-ice model instead of a fully coupled model like Holland et al.¹³ did. Morioka et al.¹⁵ used observed sea-ice initial conditions and compared with observations, while Marchi et al.¹⁴ and Holland et al.¹³ were perfect model studies.

In October 2021 the Australian Bureau of Meteorology (BoM) upgraded the Australian Community Climate and Earth System Simulator – Seasonal (ACCESS-S) from version S1 to S2. While the base model remained the same, the change in version was focused on using ocean, sea-ice and land initial conditions generated by the BoM instead of depending on the UK Met Office. Crucially, compared to ACCESS-S1, ACCESS-S2

139 does not assimilate sea-ice observations, so sea ice is only affected by the ocean and
140 atmospheric data assimilation via the coupled integration.
141

142 Since model configuration is identical between ACCESS-S1 and ACCESS-S2, they
143 form a sort of “opportunistic experiment” where the same forecasting model was run
144 over a long period of time with multiple ensemble forecasts initialised throughout the
145 year, with the only difference being the initial conditions. This provides an opportunity
146 to test the effect of sea-ice initial conditions on the forecast of sea-ice concentrations
147 and the climate.
148

149 In this study we compare sea-ice hindcasts produced by ACCESS-S1 and ACCESS-S2.
150 We focus on seasonality of errors and biases and the effect of the data assimilation
151 system. This comparison will inform future work with the prediction system as a
152 research tool to better understand the dynamics and variability of the Antarctic sea
153 ice and its impacts on the climate system as well as to explore the potential of using
154 its sea-ice forecasts for decision-making. The work will also serve as a benchmark for
155 future prediction systems to attempt to improve upon.
156

166 **Data and methods**

167 **ACCESS-S2**

168 ACCESS-S2¹⁶ is the Bureau of Meteorology’s seasonal forecast system which became
169 operational in October 2021, replacing the ACCESS-S1 system¹⁷. The model com-
170 ponents of both ACCESS-S2 and ACCESS-S1 are identical with the same numbers
171 of levels and resolution. They consist of the Global Atmosphere 6.0 (GA6)^{18;19}, the
172 Unified Model’s Global Land 6.0^{19;20}, NEMO Global Ocean 5.0^{21;22} and Global Sea
173 Ice 6.0 [CICE; Rae et al. ²³]. The atmosphere has a N216 horizontal resolution (~60 km
174 in the mid-latitudes) with 85 vertical levels. The land model uses the same horizontal
175

grid as the atmosphere with four soil levels. The ocean component has a nominal horizontal resolution of $1/4^\circ$ with 75 vertical levels. The sea-ice component, based on CICE version 4.1, has the same resolution as the ocean component and five sea-ice thickness categories as well as an open water category. 185
186
187
188
189
190
191
192
193
194
195
196
197
198
199
200
201
202
203
204
205
206
207
208
209
210
211
212
213
214
215
216
217
218
219
220
221
222
223
224
225
226
227
228
229
230

Both systems take atmospheric initial conditions derived from ERA-interim²⁴ for their hindcasts. The main difference between the hindcasts of the two systems are the ocean and sea-ice initial conditions. ACCESS-S1's ocean and sea-ice initial conditions come from the Met Office FOAM system, which uses a multivariate, incremental three-dimensional variational (3D-Var), first-guess-at-appropriate-time (FGAT) data assimilation scheme²⁵ and assimilates sea surface temperature (SST), sea surface height (SSH), in situ temperature and salinity profiles, and satellite observations of sea-ice concentration using the EUMETSAT OSISAF product described in the next section. ACCESS-S2, on the other hand, is initialised from ocean conditions generated by the BoM weakly coupled ensemble data assimilation scheme described in Wedd et al.¹⁶. This scheme uses an optimal interpolation method and assimilates temperature and salinity profiles from EN4²⁶. SSTs are nudged to Reynolds OISSTv2.1²⁷ in areas where SSTs are over 0°C and Sea Surface Salinity is weakly nudged to the World Ocean Atlas 2013 climatology²⁸.

Of most relevance for this work, sea-ice concentrations are not assimilated in ACCESS-S2. Assimilation cycles are performed daily. The coupled model runs for 24 hours initialised from the previous cycle. Then the restart file fields of the ocean component are used as first guess in the data assimilation cycle and the innovations are used to build the next ocean initial conditions for the following cycle. The atmosphere fields from that daily integration are not used and instead the model atmosphere is initialised using ERA-Interim. The sea-ice initial conditions for the next cycle are the unaltered output of the previous daily integration. Then the cycle starts again and the coupled model runs for another 24 hours. During this integration the sea-ice component is

231 affected by the ocean innovations and the new atmosphere initial conditions via the
232 coupler.

234
235 The ACCESS-S1 hindcast set is made up of nine members created by perturbing the
236 atmospheric fields only with a random field perturbation¹⁷ and runs for 217 days for
237 the period 1990–2012 initialised at the first of every month. The ACCESS-S2 hindcast
238 set used in this study runs for the period 1981–2018. Ensemble members are created in
239 the same manner as ACCESS-S1 members, however, due to computing cost limitations,
240 only three members per forecast initialisation date were run for 279 days. Bigger
241 ensembles were generated by aggregating several three-member ensembles initialised
242 on successive days¹⁶. Here, we build a nine-member time-lagged ensemble from three
243 consecutive three-member forecasts initialised at the first of every month and the two
244 previous days and run for 279 days. We analyse the ensemble mean hindcasts unless
245 otherwise specified.

246
247 Anomalies for each hindcast set are taken with respect to their own climatology specific
248 to each initialisation date and forecast lead time, for the period 1990–2012. This serves
249 as a first-order correction of model bias and drift. For monthly means, we define “0
250 lead time months” as the monthly mean forecast of the same month of initialisation.
251
252 Besides sea-ice concentration, we also analyse mean sea-ice thickness, which we compute
253 as total sea-ice volume divided by total sea-ice area.

254

255

256 **Verification datasets**

257

258 For verification we use satellite-derived sea-ice concentration, which estimates the
259 proportion of each grid area that is covered with ice. Datasets derived using different
260 algorithms and satellite platforms, each have their own biases and uncertainties.
261 Estimates of inter-product uncertainty of sea-ice extent (SIE, defined here as the total
262 region of the Southern Ocean with at least 15% sea-ice cover) are of the order of 0.5
263
264

million km^2 ²⁹. As will be shown below, this spread is minimal compared with the typical errors in the ACCESS-S2 and ACCESS-S1 forecasts, so the overall conclusions of this study are independent of the verification dataset used.

We use NOAA/NSIDC's Climate Data Record V4 [CDR; Meier et al.³⁰] as the primary sea-ice verification dataset. It takes the maximum value of the NASA Team³¹ and NASA Bootstrap³² sea-ice concentration products to reduce their low concentration bias^{30;33}. Both source algorithms use data from the Scanning Multichannel Microwave Radiometer (SMMR) on the Nimbus-7 satellite and from the Special Sensor Microwave/Imager (SSM/I) sensors on the Defense Meteorological Satellite Program's (DMSP) -F8, -F11, and -F13 satellites. The data have a spatial resolution of 25 by 25 km and daily from November 1978 onwards.

The European Organisation for the Exploitation of Meteorological Satellites (EUMETSAT) Ocean and Sea Ice Satellite Application Facility [OSI; EUMETSAT Ocean and Sea Ice Satellite Application Facility³⁴] based on the SSMIS sensor is another satellite-derived sea-ice concentration product. It is based on mostly the same sensors as the NOAA CDR but computed independently using different algorithms. Figures prepared with this dataset are provided in the supplementary material and do not differ significantly from the ones prepared using CDR.

Error measures

For evaluation purposes, we use a series of measures. Sea-ice extent is defined as the area of the ocean at least 15% covered by sea-ice. This threshold is motivated by the limitations in satellite retrieval, which is increasingly unreliable for lower sea-ice concentrations³⁵.

Pan-Antarctic (net) sea-ice extent serves as a hemispheric measure of the amount of sea ice, but it does not take into account the spatial distribution. A model could have

323 a relatively accurate extent of the net ice but with different regional distributions. To
 324 account for location errors, we computed the Root Mean Squared Error (RMSE) of
 325 grid-point sea-ice concentration anomalies.
 326
 327 We compute RMSE as the square root of the area-averaged squared differences between
 328 grid-point forecasted and observed sea-ice concentration anomalies. We compute a
 329 pan-Antarctic RMSE by averaging over the whole NOAA/NSIDC CDRV4 Southern
 330 Hemisphere domain, and also a zonally-varying RMSE computed over 15 longitude
 331 slices 24° wide around Antarctica.
 332
 333 All error measures were computed on the NOAA/NSIDC CDRV4 domain grid, to
 334 which model output was bilinearly interpolated. Note that the ACCESS CICE model
 335 grid has resolution between two and three times higher than NOAA/NSIDC CDRV4.
 336
 337 Forecast errors are also compared with hypothetical forecasts based on the persistence
 338 of anomalies and on climatology. The persistence forecast is generated by extending
 339 the observed sea-ice concentration anomalies the day of the forecast initialisation and
 340 comparing it with the actual anomalies observed. The climatological forecast error is
 341 computed as the standard deviation of daily anomalies.
 342
 343 As a measure of forecast improvement over the hypothetical forecast, we use the skill
 344 score³⁶, defined as
 345
 346

$$S = 1 - \frac{RMSE_f}{RMSE_r}$$
 347
 348 Where $RMSE_f$ is the RMSE of the forecast, $RMSE_r$ is the RMSE of the reference
 349 forecast. Negative skill score indicates that the forecast is worse than the reference
 350 forecast while positive values indicate an improvement. A perfect forecast would have
 351 zero RMSE and thus a skill score of 1.
 352
 353

Computational procedures

369

370

371

372

373

374

375

376

377

378

379

380

381

382

383

384

385

386

387

388

389

390

391

392

393

394

395

396

397

398

399

400

401

402

403

404

405

406

407

408

409

410

411

412

413

414

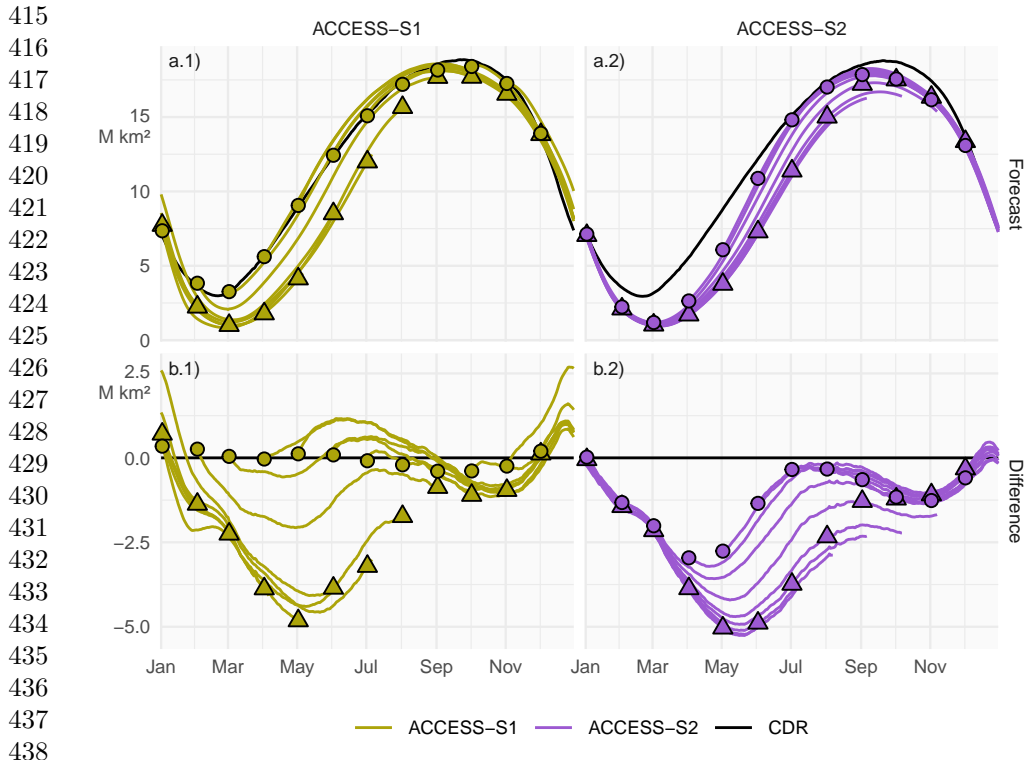
We performed all analyses in this paper using the R programming language³⁷, using data.table³⁸ and metR³⁹ packages. Significant processing was performed using the CDO command line operators⁴⁰. All graphics are made using ggplot2⁴¹. The paper was rendered using knitr and Quarto^{42;43}.

Results and discussion

Bias

Figure 1 shows mean sea-ice extent of the ACCESS-S1 and ACCESS-S2 hindcasts (row a) and their differences from mean sea-ice extent of NOAA/NSIDC CDRV4 (row b). Mean extent at the first of every month is indicated with circles for the initial conditions and with triangles for the longest lead time possible for each model (between 274 and 277 days for ACCESS-S2 and between 213 and 216 days for ACCESS-S1). At this long lead time, information of the initial conditions is essentially lost and the forecast reverts close to each model's preferred equilibrium state.

ACCESS-S2 initial conditions (circles in Fig. 1 column 2) show an overall negative bias, especially in the late summer-early autumn, while ACCESS-S1 initial conditions (circles in Fig. 1 column 1) are very close to observations, as expected from the assimilation of sea-ice observations to produce the initial conditions of ACCESS-S1. Both systems' equilibrium states (triangles) show negative biases of sea-ice extent, particularly in the growth phase of late-autumn and winter months. This is due primarily to the melt season being longer than in observations and with faster melt between January and March and the growing seasons being shorter with slower growth during March and April. This is then followed by faster growth between May and July (Figure 2). Many sea-ice models exhibit this systematic underestimation during the sea-ice minimum



439 **Figure 1:** Row a: Pan-Antarctic daily mean sea-ice extent for all hindcasts initialised
440 on the first of each calendar month for ACCESS-S1 (column 1; green) and ACCESS-S2
441 (column 2; purple). Observed mean sea-ice extent in each corresponding hindcast period
442 is shown in black. Row b: Mean differences between the forecast and the observed
443 values. Circles represent the initial conditions at the start of forecasts (i.e., the first of
444 every month), and triangles represent the mean values at the lead time corresponding
445 to the maximum lead time in S1 (between 213 and 216 days, depending on the month)
446
447

448 and early freezing season⁸, which could indicate problems in the representation of
449 thermodynamics in the model⁶. It is also not surprising that both forecasting systems
450 converge to a similar equilibrium state because they share the same model formulation.
451
452 The difference between the initial conditions (circles) and the model equilibrium
453 state (triangles) can be mostly attributed to the effect of data assimilation, which
454 in ACCESS-S2 is due solely to the coupling of sea-ice with the atmosphere and the
455 ocean. From May to October, in ACCESS-S2 circles are closer to observations than
456
457
458
459
460

the triangles are, indicating that the information from the ocean and atmosphere data assimilation is affecting sea ice and improving the initial conditions. During these months, ACCESS-S1 can overestimate the sea-ice extent at short lead time. For the rest of the year circles are overlaid with triangles in ACCESS-S2, indicating that the ocean and atmosphere data assimilation is not affecting sea ice and that this component of the model is virtually free-running.

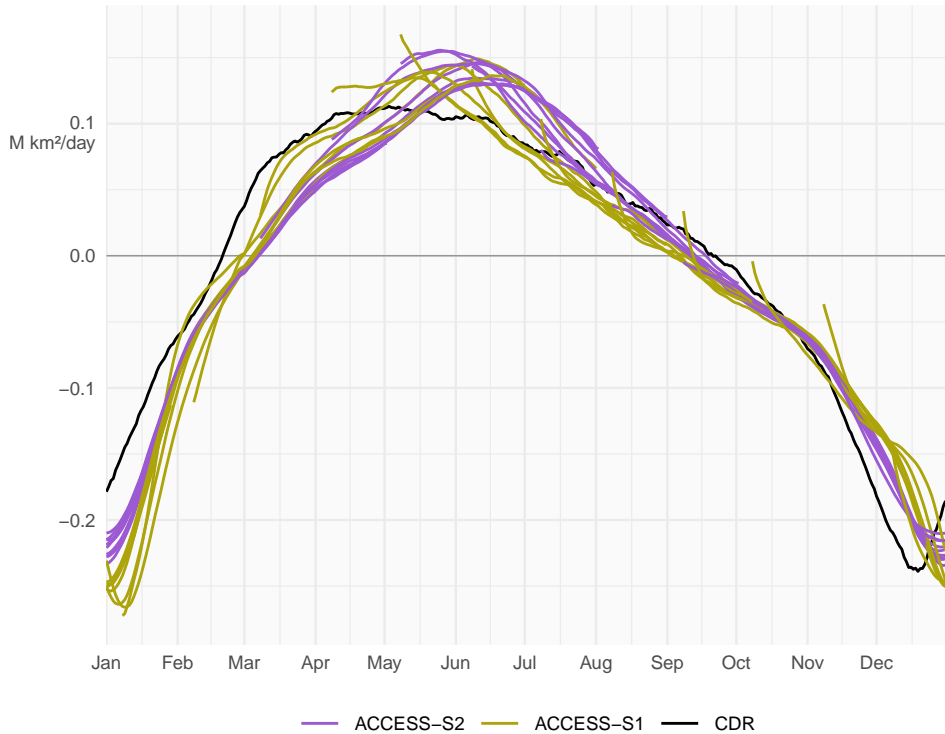
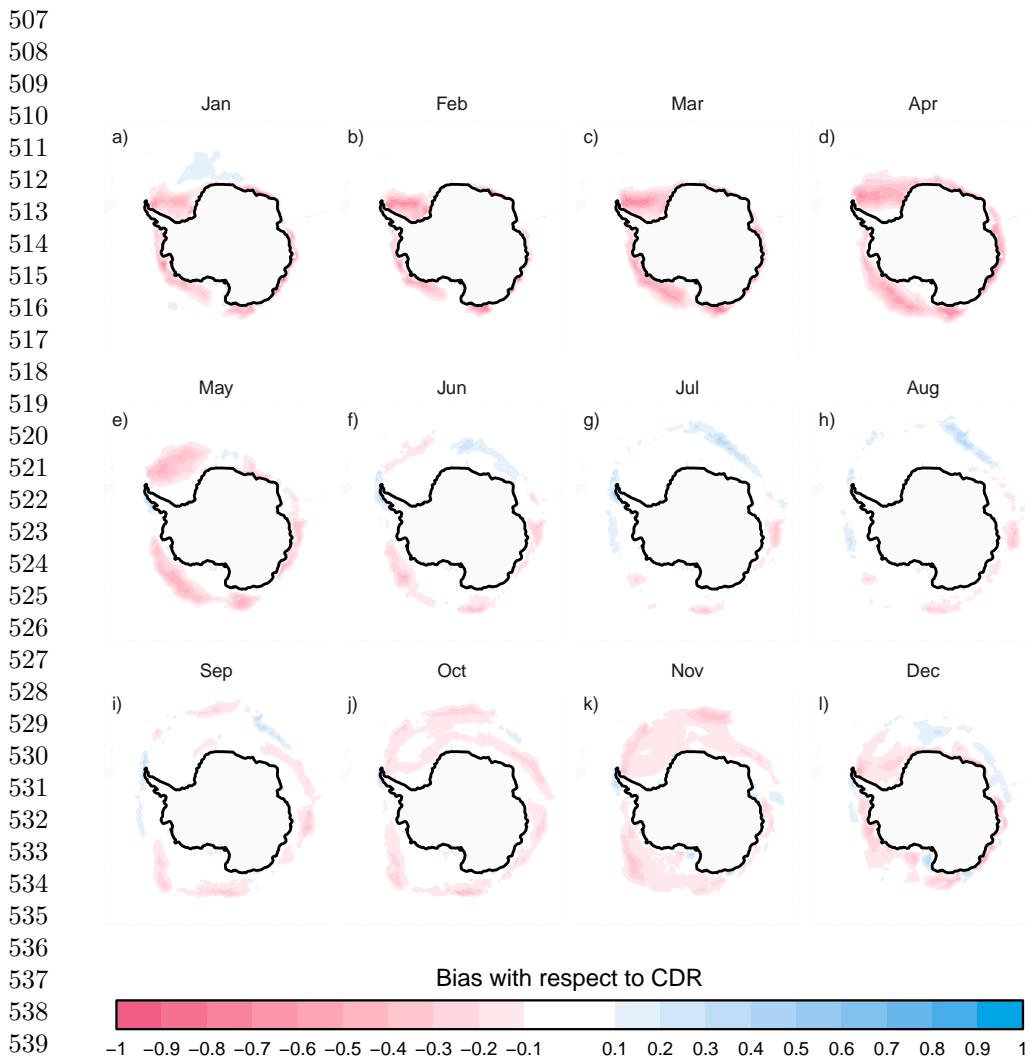


Figure 2: Mean daily sea-ice extent growth ($10^6 \text{ km}^2/\text{day}$) in ACCESS-S1 (green) and ACCESS-S2 (purple) hindcasts and observations (black), computed as the mean daily differences in sea-ice extent between each date and the next for each forecast month. Values are smoothed with a 11-day running mean.

To further understand the bias in ACCESS-S2, Figure 3 shows spatial patterns of the differences of monthly mean sea-ice concentrations between NOAA/NSIDC CDRV4 and ACCESS-S2 hindcasts at the shortest monthly lead time. From October to May,



543 **Figure 3:** Ensemble mean difference between monthly sea-ice concentration of
 544 ACCESS-S2 ensemble mean forecast at 0-month lead time (monthly mean values fore-
 545 casted from the forecast initialised at the first of the month) and observations (CDR).

546
 547
 548 the model underestimates sea-ice concentrations in most regions except for the inner
 549 Weddell Sea in April and May, where sea-ice concentrations saturate to 1 both in
 550 the observations and forecasts. In winter, the differences are limited to a narrow
 551
 552

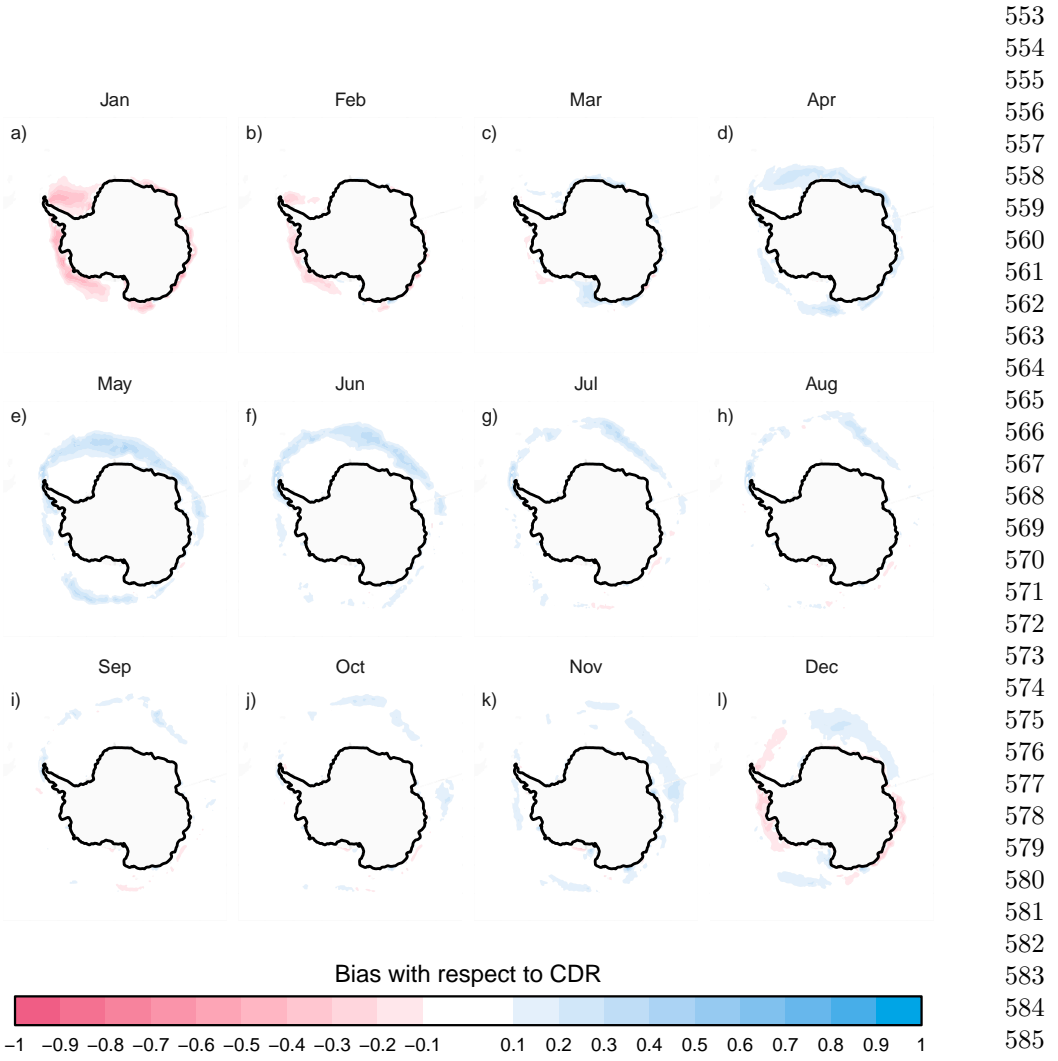


Figure 4: Same as Figure 3 but for ACCESS-S1.

band around the sea-ice edge with slight positive biases in the African sector of East Antarctica and negative biases around the Indian Ocean sector which partially compensate, resulting in the near-zero extent bias seen in those months (Figure 1).

599 ACCESS-S1 has a comparatively smaller overall bias (Figure 4). The largest values are
600 found between April and June, when the faster growth results in large positive bias
601 along the sea-ice edge, and in January, when the faster melt leads to large negative
602 bias in the Weddell and Amundsen Seas.
603

604

605

606

607 RMSE

608

609

610 Figure 5 shows monthly sea-ice extent anomalies forecasted at selected lead times.
611 Compared with ACCESS-S1, ACCESS-S2 anomaly forecasts are relatively poor (large
612 RMSE) even for the first month (lead time 0), whereas ACCESS-S1 forecasts stay
613 relatively skilful even at a lead time of three months. ACCESS-S2 shows much larger
614 interannual variability than observations, with dramatic lows between 1995 and 2007,
615 and highs between 2007 and 2015.
616

617

618 Unexpectedly, for ACCESS-S2, RMSE improves with lead time, even though the cor-
619 relation degrades with lead time. This is puzzling behaviour that goes contrary to
620 what is usually seen in prediction models. The explanation seems to be the mentioned
621 increased interannual variability. Figure 6 shows the interannual standard deviation
622 of monthly sea-ice extent of the forecasts as a function of lead time compared with
623 observations. ACCESS-S1 standard deviation lies within the observed standard devia-
624 tion regardless of lead time, while ACCESS-S2 standard deviation is more than twice
625 that of observations at zero lead time and only approaches the observed value at nine
626 months lead time for most months.
627

628

629 ACCESS-S2 forecasts of sea-ice extent anomalies seem to align moderately well with
630 observations (leading to moderately high correlation) but their magnitude is overesti-
631 mated (leading to large errors). This could be caused by ACCESS-S2 sea ice being much
632 more sensitive to atmospheric and oceanic forcing, perhaps due to lower thickness.
633

634

635

636

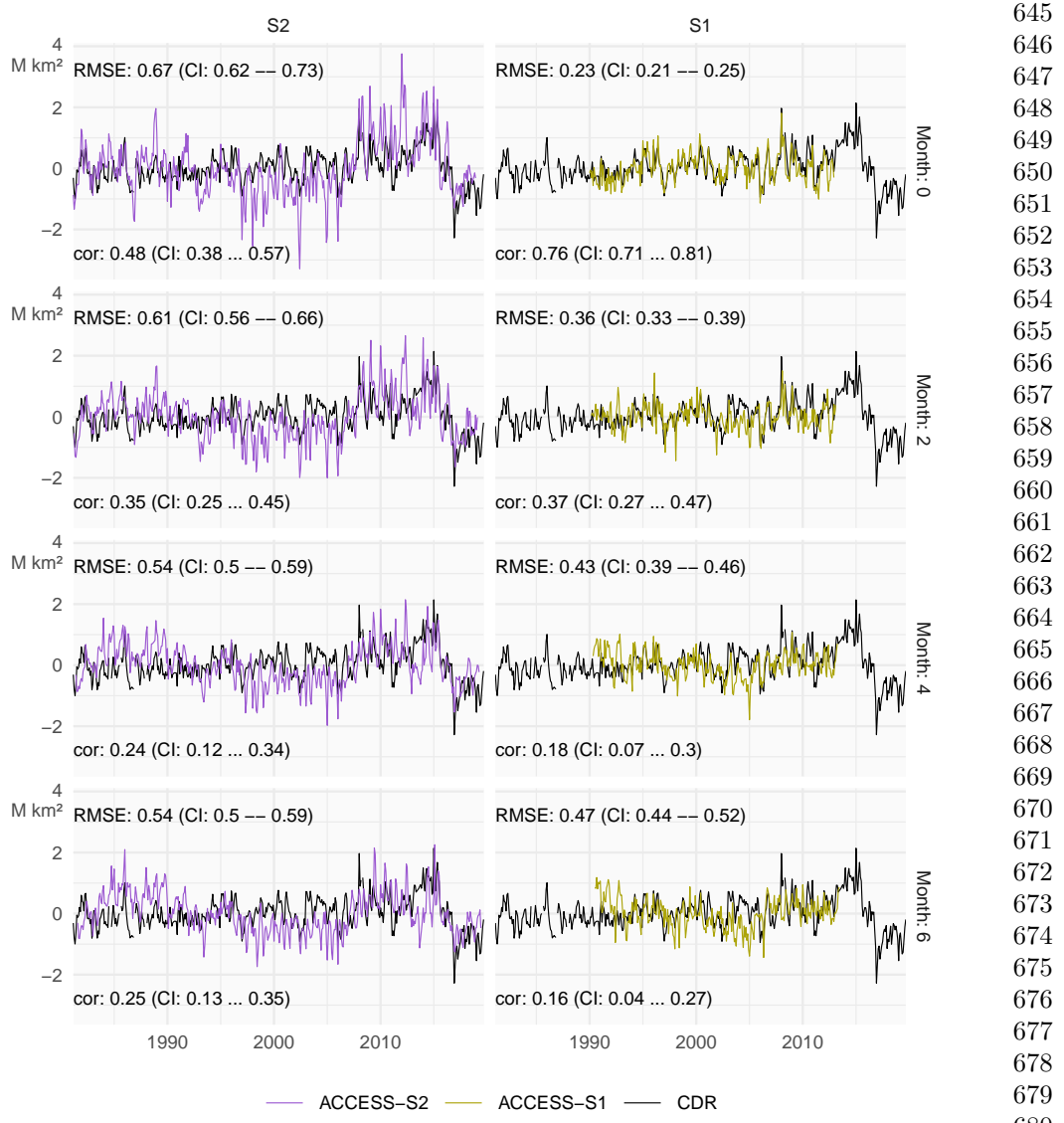


Figure 5: Monthly mean sea-ice extent anomalies of the observations (black) and forecasts from ACCESS-S1 (right column; purple) and ACCESS-S2 (left column; green) at lead times of 0, 2, 4, and 6 months. The RMSE and correlation during the overlapping period of ACCESS-S1 and ACCESS-S2 hindcasts (1990–2013) are shown on the top left and bottom left of each panel respectively.

As an example, Figure 7 shows sea-ice concentration anomalies (top row) and sea-ice thickness and the difference between the two models (bottom row) for 2 May

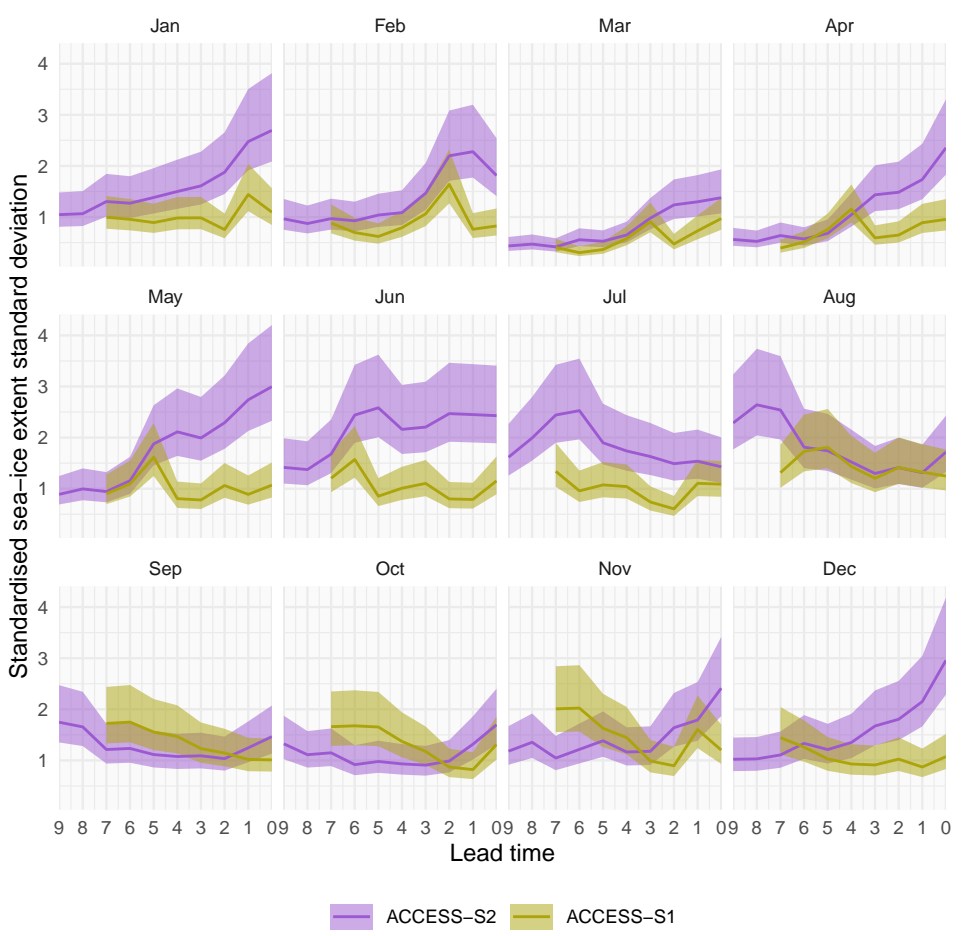


Figure 6: Interannual standard deviation with 95% confidence interval of monthly mean sea-ice extent forecasted for each month divided by that month's sea-ice extent observation standard deviation. ACCESS-S1 and ACCESS-S2 at different lead times. Each panel indicates the target month. Note the reverse horizontal axis.

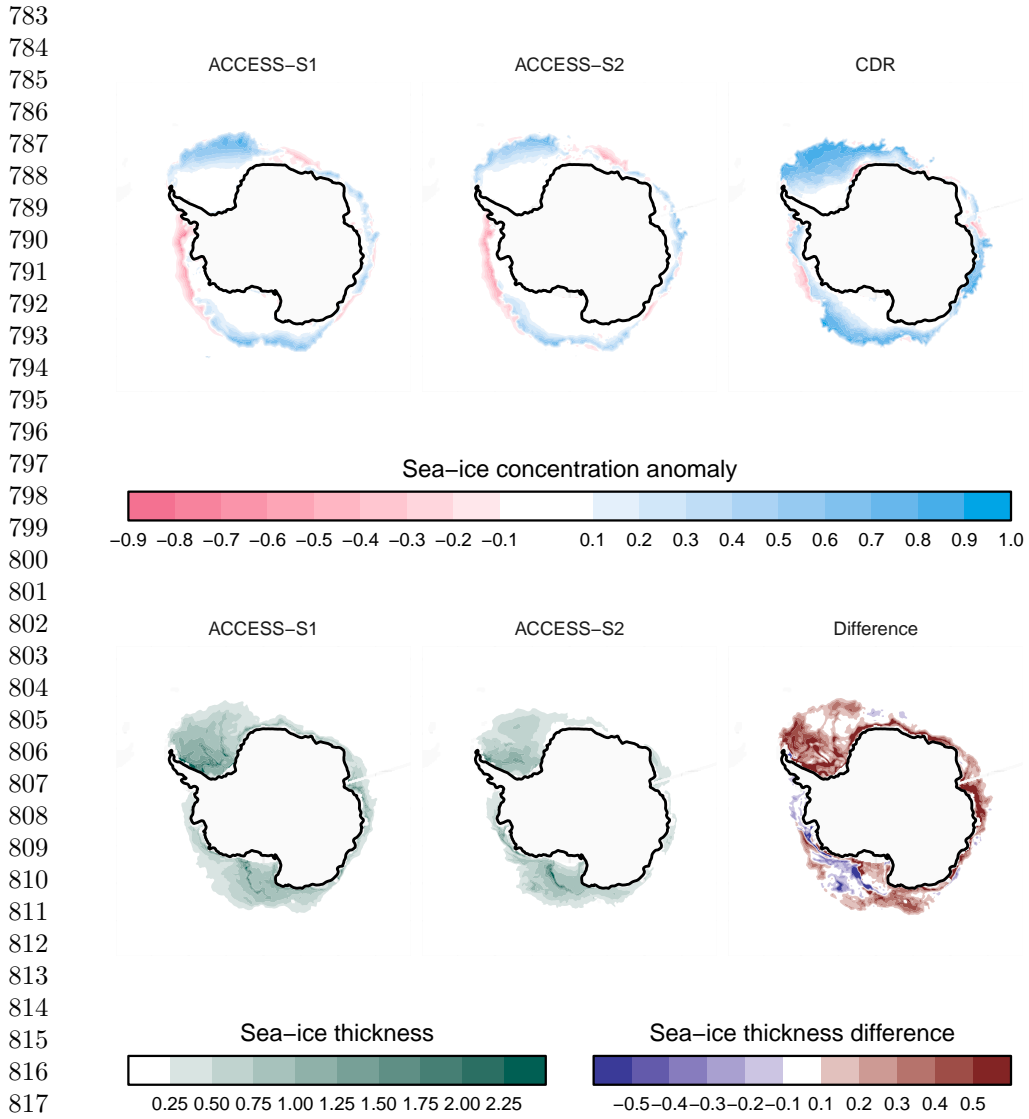
2008 initialised one day prior; being that close to initialisation date, these are very approximately the initial conditions. ACCESS-S1 sea-ice concentrations anomalies are very close to observations as expected from the system assimilating these data. ACCESS-S2 sea-ice concentration anomalies, which are not assimilated, are not as close, but the large-scale pattern is aligned with observations. The system simulates large positive anomalies in the Weddell and Ross Seas and slight negative anomalies

in the Amundsen and Bellingshausen Seas. The fact that ACCESS-S2 can simulate
this pattern without assimilating sea-ice data suggests that atmospheric and oceanic
forcing were the dominant drivers. However, the magnitude of the sea-ice anomalies is
too big. It is plausible that this is due to the thinner ice simulated by ACCESS-S2
(bottom row).

Extending beyond the one case in Figure 7, Figure 8 shows monthly mean sea-ice
thickness as a function of lead time for ACCESS-S1 and ACCESS-S2. Supporting the
idea that thinner ice is what causes the increased extent variability in ACCESS-S2,
this system simulates thinner sea-ice compared to ACCESS-S1 overall at almost all
lead times and in all months except for summer at short lead times (Dec-Jan, 0-1
months; Feb-Mar, 0-2 months). However, in both systems, forecasted sea-ice is thicker
at shorter lead times and then decreases, particularly in the summer months. If thinner
ice were a sufficient cause of increased variability, then we would expect variability to
increase with lead time in both forecasting systems.

The fact that ACCESS-S1 and ACCESS-S2 share the same model configuration and
that the increased variability is more extreme at short lead times (Fig. 6) suggests
that the data assimilation procedure is partly responsible. It is possible that sea-ice in
the ACCESS-S2 system is left in an unbalanced state after assimilating atmospheric
and oceanic data but not sea-ice data, leading to large responses that are amplified
by the thin ice in the initial states which then subside at longer lead times when the
model is balanced.

To assess ACCESS-S2 forecasts in more detail, we compute error measures for all
hindcasts started on the 1st of every month. Figure 9 shows the mean RMSE of sea-ice
concentration anomalies for ACCESS-S1 and ACCESS-S2 hindcasts compared against
persistence and climatological forecasts used as a benchmark. Due to errors in the
initial conditions, it is expected that persistence forecasts would be better than the
model forecasts at very short lead times, but that the persistence forecast errors would



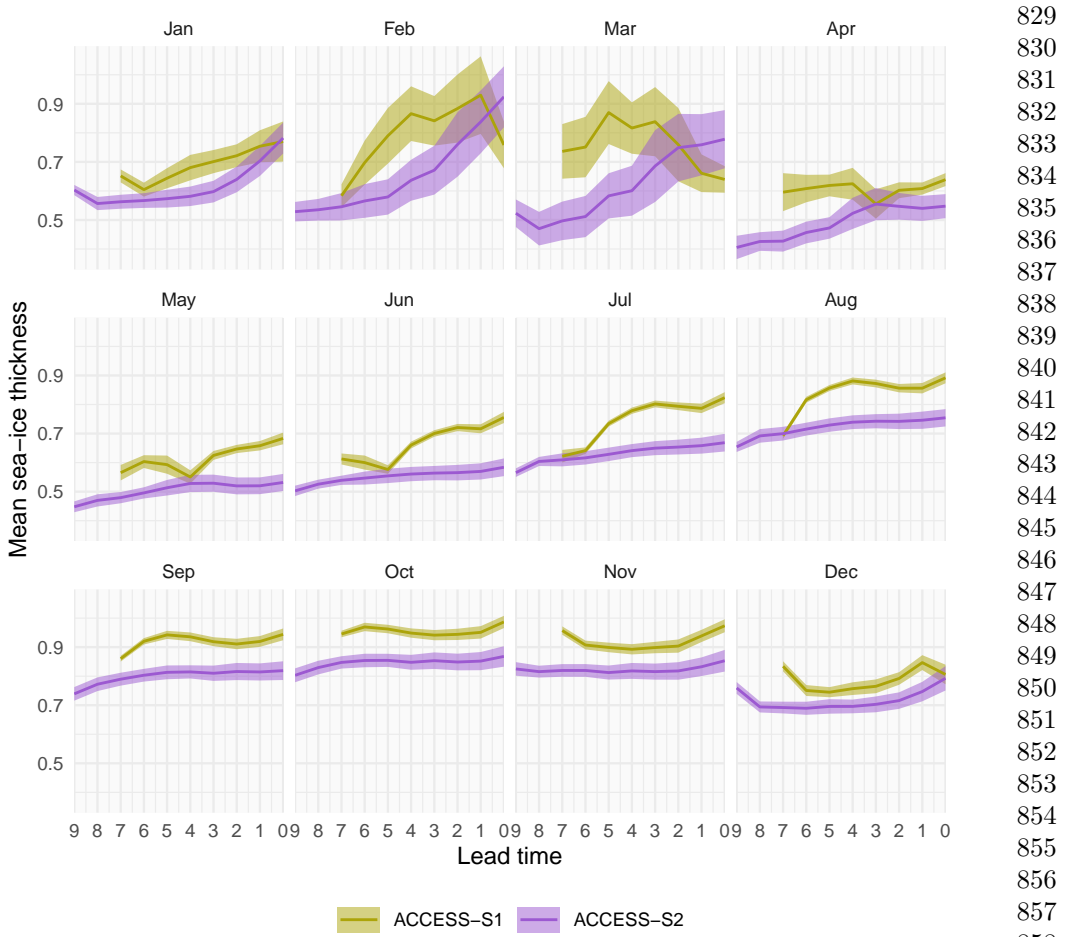
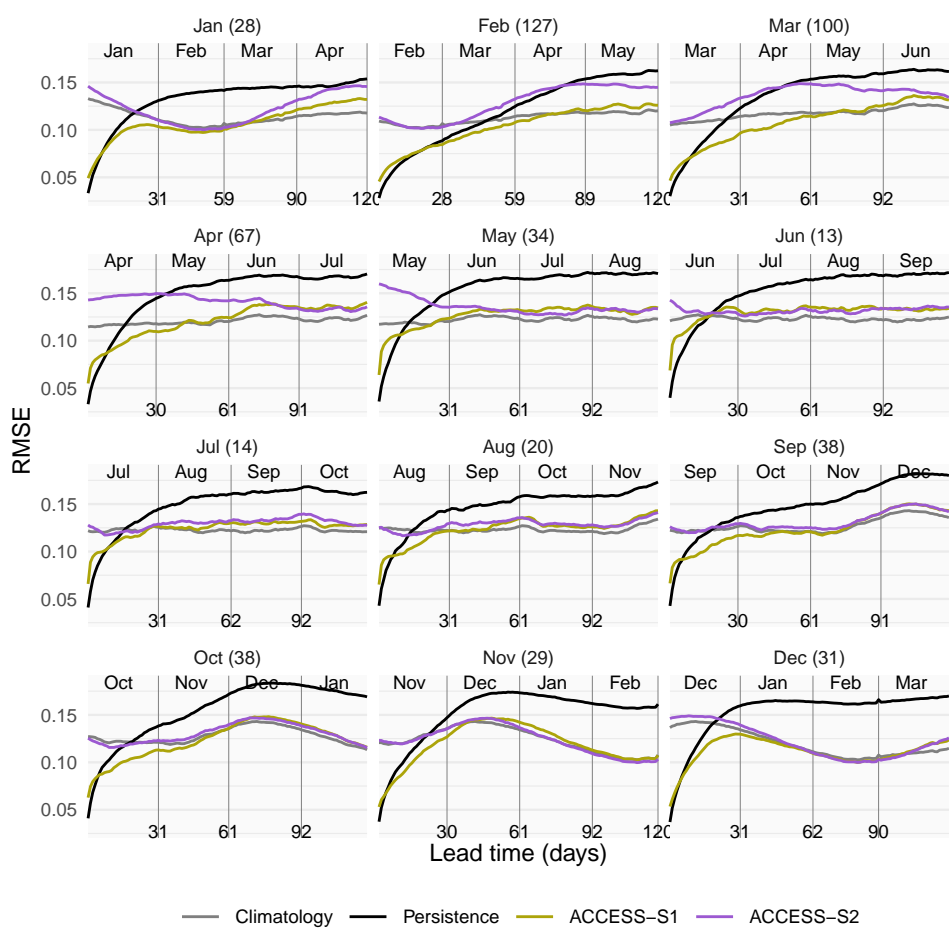


Figure 8: Mean and 95% interval of monthly mean sea-ice thickness for ACCESS-S1 and ACCESS-S2 at different lead times. Each panel indicates the target month. Note the reverse horizontal axis.

about 30 days for most months except for February, when it grows much slower. The ACCESS-S1 forecast errors grow slower than persistence forecast errors and remain lower after less than 10 days on average. The ACCESS-S2 forecast error starts high in all months and is lower than the persistence forecast error after more than 15 days in most months except for forecast initialised in February, when it takes 80 days.



905 **Figure 9:** Mean RMSE of sea-ice concentration anomalies as a function of forecast
906 lead time for all forecasts initialised on the first of each month compared with a
907 reference forecast of persistence of anomalies (black) and climatology (gray). Only the
908 first 120 days are shown. In parentheses, the shortest time at which ACCESS-S1 and
909 ACCESS-S2 mean RMSE is not statistically different at the 99% confidence level.

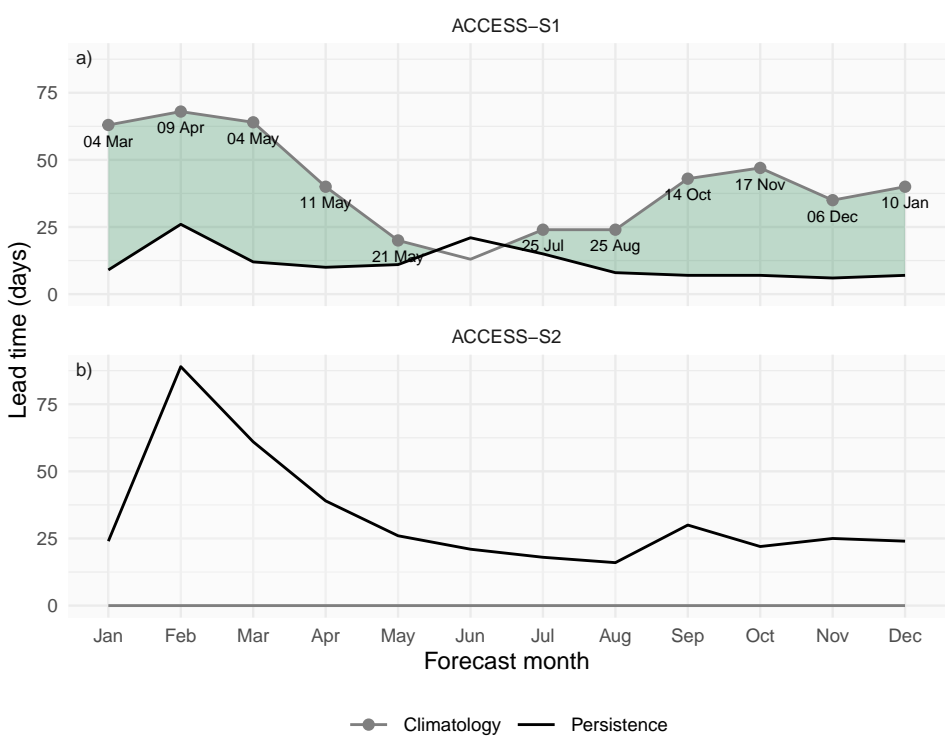
910
911
912 At longer lead times, it is more appropriate to compare errors with the climatological
913 forecast error. The lead time at which ACCESS-S1 forecast error is higher than
914 the climatological forecast error varies between more than 60 and less than 20 days
915 depending on forecast initialisation month with the minimum in June. ACCESS-S2
916
917
918
919
920

forecasts never have lower error than climatology, on the other hand, except marginally
in October forecasts. 921
922
923

Figure 10 summarises the lead time window in which each hindcast is better than
both the persistence forecast and the climatological forecast as a function of forecast
month. ACCESS-S1 forecasts have a wider lead time window in the summer than
the other seasons and is not better than both benchmarks at forecasting June sea-ice
concentration anomalies. Forecasts initialised in May and June are particularly poor,
and July cannot be forecasted better than the benchmarks. This is consistent with
the mid-winter loss of predictability observed by Libera et al.⁴⁴, who attributed it to
deep warm water entraining into the mixed layer. 924
925
926
927
928
929
930
931
932
933
934
935
936
937
938
939
940
941
942
943
944
945
946
947
948
949
950
951
952
953
954
955
956
957
958
959
960
961
962
963
964
965
966

To analyse the spatial distribution of the model error, we computed the RMSE of
zonal mean sea-ice concentration anomalies on 15 slices of 24° longitude span for each
forecasting system. We control for some areas being naturally easier to forecast than
others by computing the RMSE skill score with the climatological forecast RMSE as
reference. 938
939
940
941
942
943
944
945
946
947
948
949
950
951
952
953
954
955
956
957
958
959
960
961
962
963
964
965
966

For ACCESS-S1 forecasts (Figure 11), skill tends to be lower off the coast of Eastern
Antarctica even at short lead times; for instance, the skill score for forecasts initialised
in May and June are negative between 0° and 120°E even at almost zero lead time.
This mirrors Libera et al.⁴⁴ findings of a “winter predictability barrier”, although they
focus on the Weddell Sea and here we show that the effect seems to be stronger more
to the east. In West Antarctica there is a hint of easterly-propagating skill in forecasts
initialised in February and March. This is consistent with Holland et al.¹³ findings
that memory of sea-ice anomalies are stored in ocean heat content anomalies that are
transported east by the Antarctic Circumpolar Current. 947
948
949
950
951
952
953
954
955
956
957
958
959
960
961
962
963
964
965
966



991 **Figure 10:** Minimum lead time at which each forecast's mean RMSE becomes larger
992 than the lower bound of the 95% confidence interval of persistence forecast RMSE
993 (black lines) and maximum lead time at which each forecast's mean RMSE remains
994 lower than the lower bound of the 95% confidence interval of climatological forecast
995 RMSE (gray lines). Green shading indicates the window where forecasts outperform
996 both persistence (lead times longer than black line) and climatology (lead times shorter
997 than gray line). Text labels show the date corresponding to the maximum lead time at
998 which each forecast outperforms climatology.
999
1000

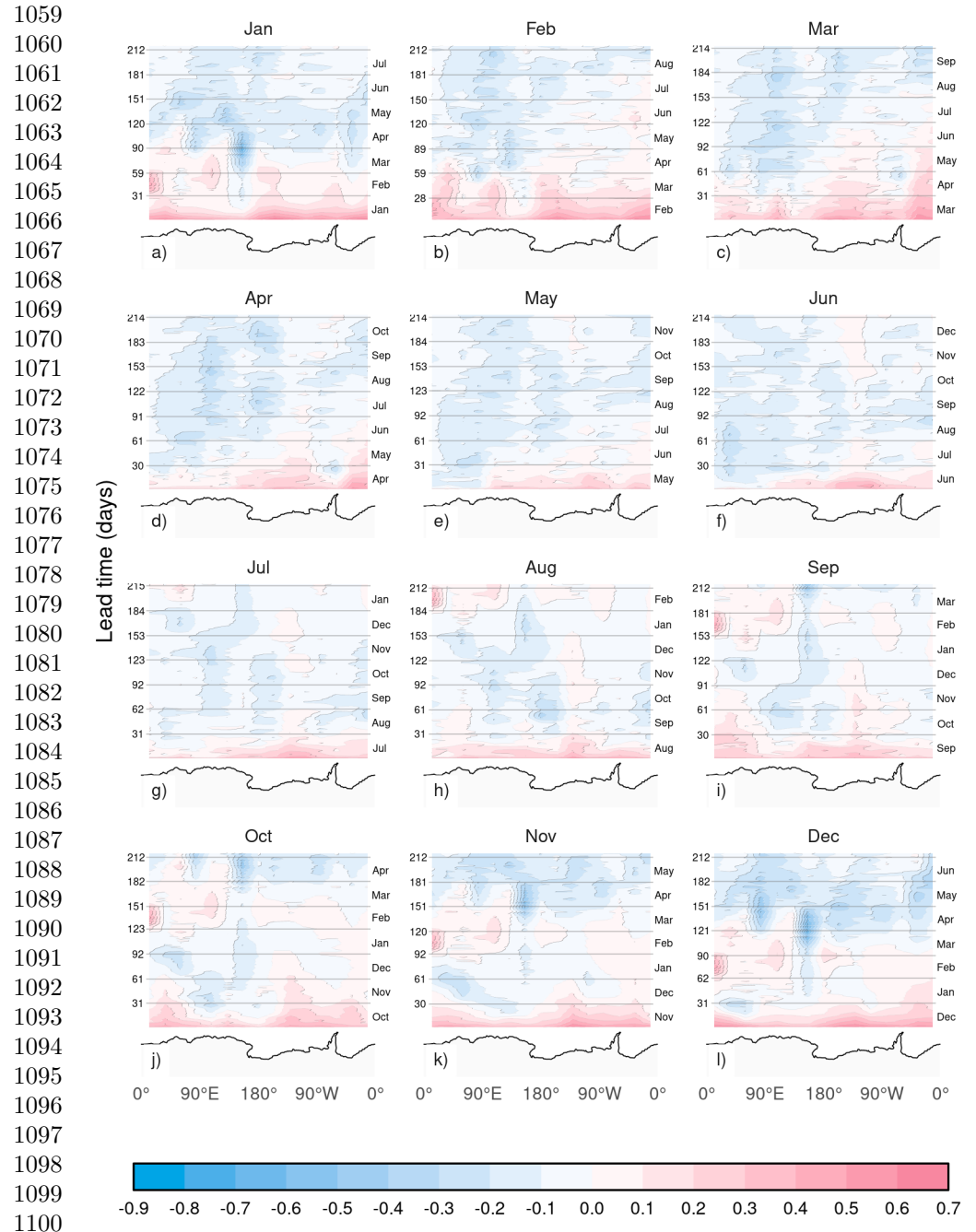
1001 times (Fig. 10), it is positive for up to a month in West Antarctica. Since oceanic and
1002 atmospheric forcing is the only source of information, this suggests that sea-ice in
1003 this region is particularly sensitive to oceanic and atmospheric forcing and suggests a
1004 role of the Pacific-South American mode and the Amundsen Sea Low to shape sea-ice
1005 concentration anomalies. The fact that this is evident in the months in which El Niño–
1006 Southern Oscillation teleconnections are more important for atmospheric circulation
1007
1008
1009
1010
1011
1012

also suggests the influence of tropical Pacific variability. February and March are the
only two months that can be forecasted with marginally positive skill in large regions.

Finally, Figure 13 shows the difference in skill between ACCESS-S1 and ACCESS-S2.
Large differences in skill indicate areas and months that are most affected by the
data assimilation present in ACCESS-S1. Between January and March, which are the
months in which ACCESS-S1 is the most skilful (Figure 10), most of the improvement
compared with ACCESS-S2 is present in the Ross and Weddell Sea. In April and May,
the improvement seems more homogeneous.

In Figure 9 the mean error was shown. Figure 14 column 1 shows the mean standard
deviation of errors among ensemble members at various lead times. At one day lead
time (Fig. 14 a.1) ACCESS-S2 has a slightly larger spread than ACCESS-S1 due
to the way that ensemble members are generated. ACCESS-S1 ensemble members
are generated by adding random field perturbations to the atmosphere only, which
then are transferred to the other components via the coupled simulation¹⁷. With this
scheme, ensemble members are all but guaranteed to be underdispersed in the ocean
and sea-ice components. The time-lag ensemble used for ACCESS-S2 ensures greater
spread. This difference is gone after about just two days, and both systems have a
comparable spread in ensemble member error afterwards (Fig. 14 b1 and c1).

Figure 14 column 2, on the other hand, shows the standard deviation of ensemble mean
error of each hindcast and the persistence forecast. At one day lead time, ACCESS-S2
ensemble mean error standard deviation is much larger than ACCESS-S1's, which in
turn is comparable to the persistence forecast error standard deviation. At longer lead
times, the spread of ACCESS-S1 and persistence forecast standard deviation increases
to eventually be comparable to ACCESS-S2 and the standard deviation in climatological
forecast errors. ACCESS-S2 error standard deviation is fairly independent of lead time
and similar to the climatological forecast error standard deviation at all lead times.



1101 **Figure 11:** RMSE skill score of ACCESS-S1 forecasts with climatological forecast as
 1102 reference computed on 15 meridional slices 24° wide as a function of lead time and
 1103 longitude. Antarctica's coastline is shown at the bottom of each panel for reference.
 1104

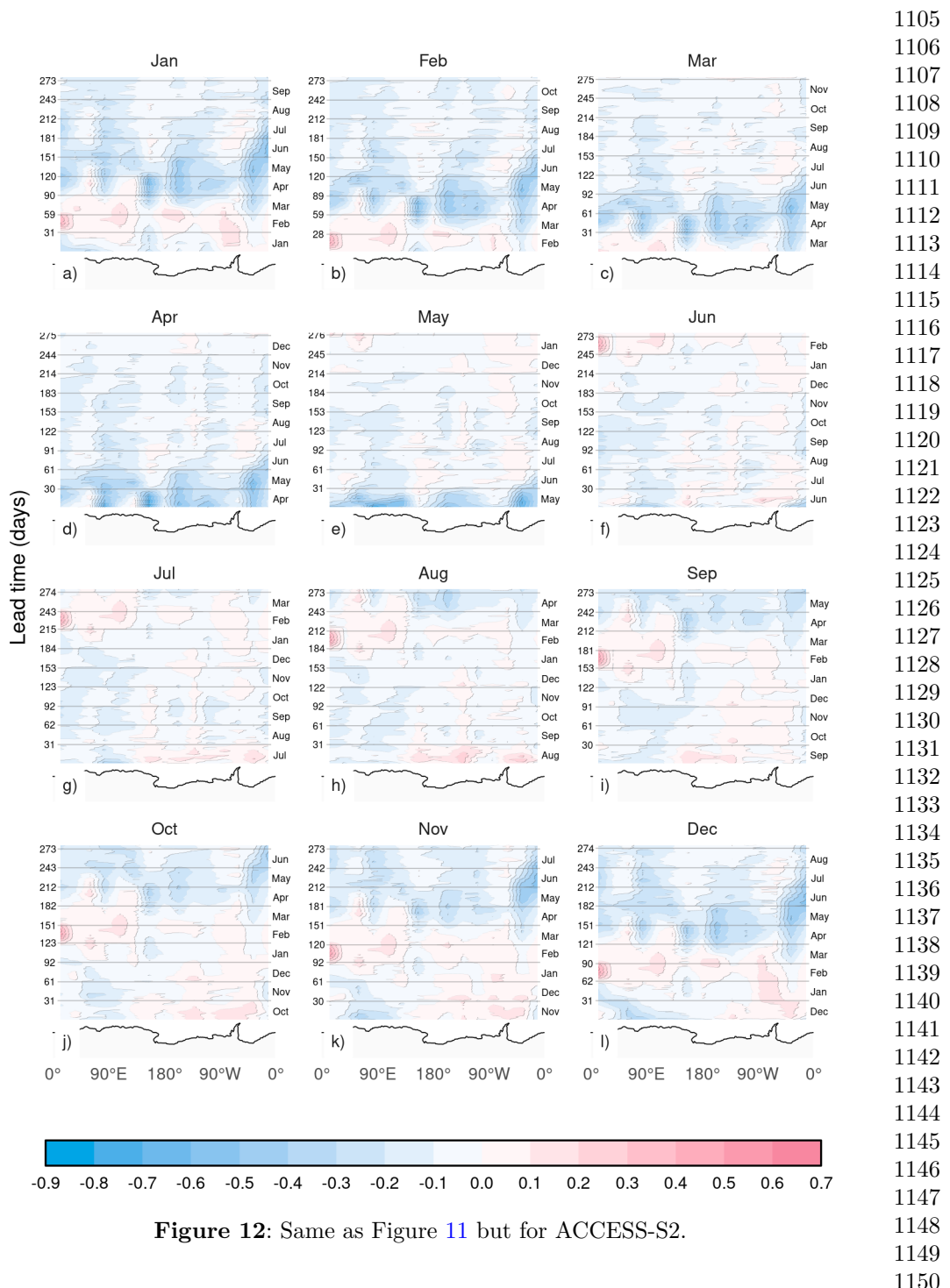
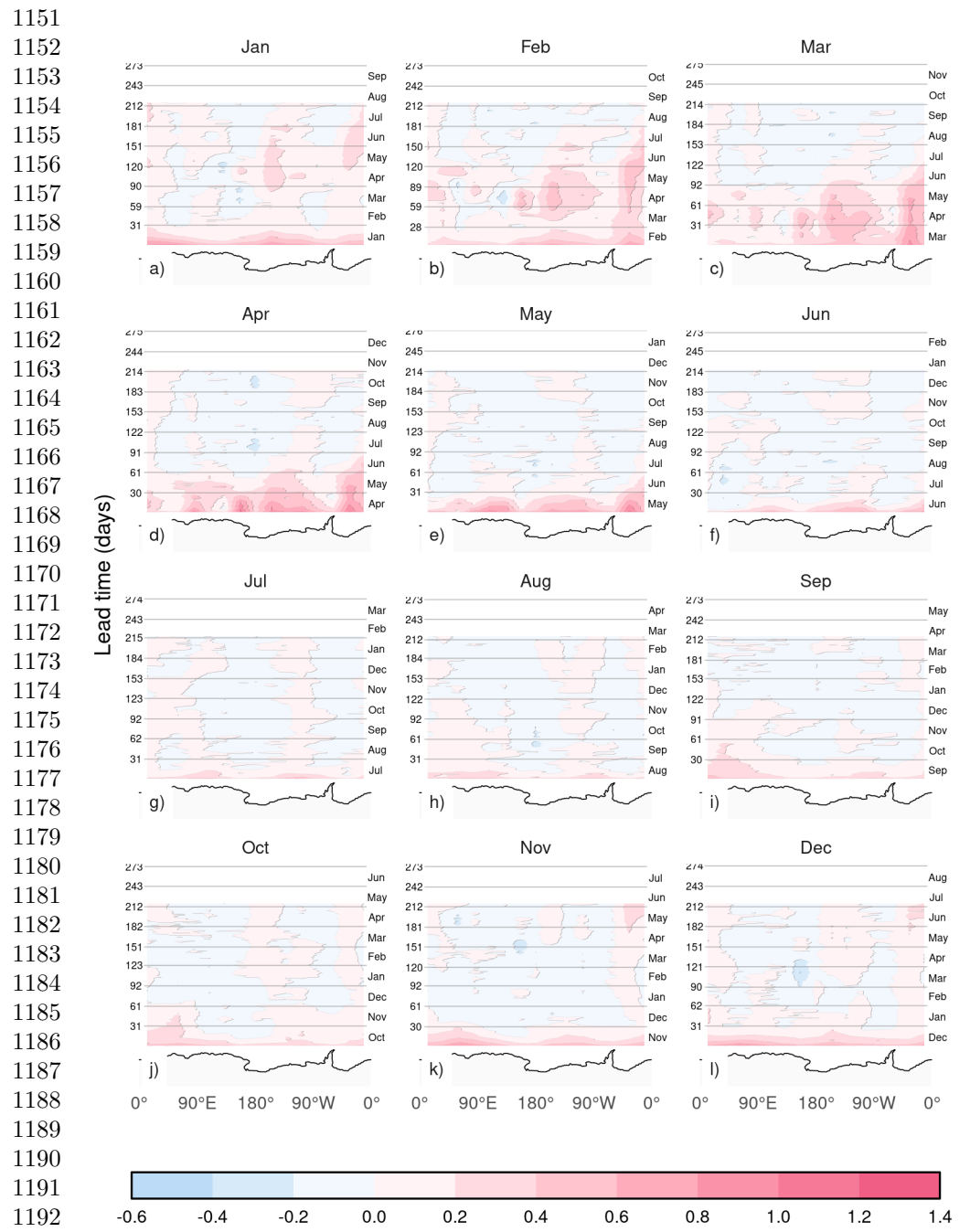


Figure 12: Same as Figure 11 but for ACCESS-S2.



1193 **Figure 13:** Same as Figure 11 but for the difference between ACCESS-S1 and ACCESS-
 1194 S2.
 1195
 1196

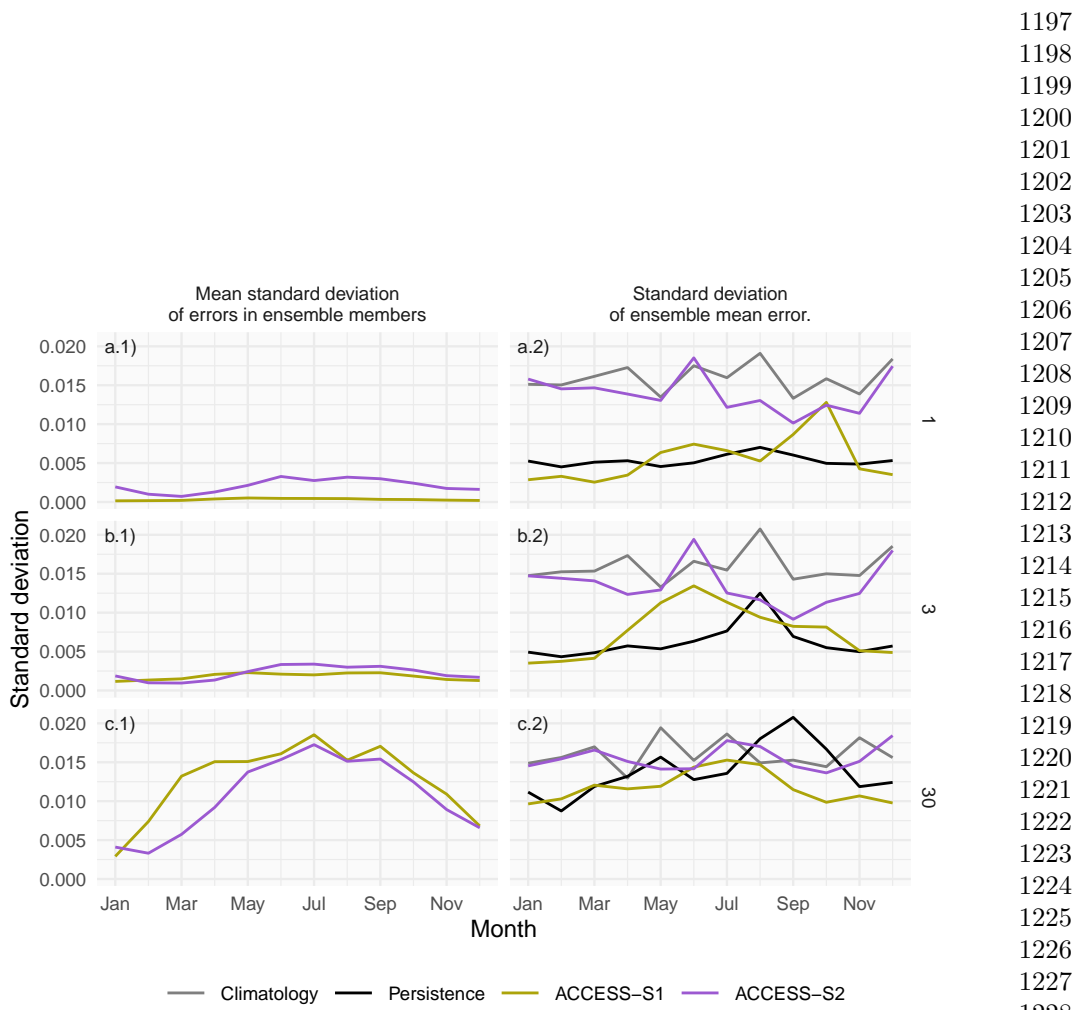


Figure 14: Decomposition of forecast error spread at 1, 5 and 30 days lead time for ACCESS-S1 and ACCESS-S2 hindcasts across initialization months. The left column shows the mean standard deviation of RMSE errors across ensemble members, while the right column shows the standard deviation of the ensemble mean RMSE error and the spread of the persistence and climatology forecasts errors.

1243 **Conclusions**

1244

1245

1246 Sea-ice forecasts from the ACCESS-S2 system show a significant low extent bias,
1247 particularly during late summer and early autumn. This bias is attributed to a faster
1248
1249 and longer melt season between January and March, and slower growth between March
1250
1251 and April. This underestimation during the minimum and early freezing season is a
1252 common issue in many seasonal-to-subseasonal (S2S) systems, suggesting potential
1253
1254 problems either with the model's thermodynamic representation or with short wave
1255
1256 radiation forcing, as shown in other climate models^{6;45}. Even though ACCESS-S2
1257 shares the same model components as ACCESS-S1, the latter does not suffer from
1258
1259 this bias, indicating that assimilating sea-ice concentrations successfully corrects for
1260
1261 the negative bias that exists in the free-running model.

1262

1263 Ensemble spread grows quickly even when perturbations are only implemented in the
1264 atmosphere component (in ACCESS-S1), indicating that sea ice is indeed responding
1265
1266 quickly to atmospheric perturbations. However, our analysis suggests that the atmo-
1267
1268 sphere and ocean data assimilation implemented in ACCESS-S2 is only effectively
1269 influencing sea-ice initial conditions from June to October, while the rest of the year,
1270
1271 the sea-ice component runs virtually free, reverting to its biased equilibrium state.
1272

1273 Zhou and Alves⁴⁶ had previously evaluated sea-ice forecasts in ACCESS-S2 and also
1274 highlighted the poor performance of this forecasting system attributed to the lack of
1275
1276 good initial conditions.

1277

1278 Analysis of the error spread shows that ACCESS-S2 initial conditions from December
1279
1280 to May not only have large errors, but that the initial error spread is very large
1281
1282 compared with ACCESS-S1. This spread is not due to the perturbation scheme, since
1283
1284 the mean error variance for individual forecasts is low and comparable with ACCESS-
1285 S1. Instead, it is due to large variance of the mean error of individual forecasts, which
1286
1287

1288

is comparable to the climatology spread. This is further evidence that individual initial
conditions are not being affected by the data assimilation scheme. 1289
1290
1291
1292
1293
1294
1295
1296
1297
1298
1299
1300
1301
1302
1303
1304
1305
1306
1307
1308
1309
1310
1311
1312
1313
1314
1315
1316
1317
1318
1319
1320
1321
1322
1323
1324
1325
1326
1327
1328
1329
1330
1331
1332
1333
1334

Although ACCESS-S1 only assimilates sea-ice concentration, it is clear that sea-ice thickness is also affected through the assimilation process. ACCESS-S1 simulates significantly thicker ice than ACCESS-S2 and in both systems sea-ice is thicker at shorter lead times than at longer lead times. Both the explicit data assimilation in ACCESS-S2 and the effects of atmospheric and oceanic data assimilation in ACCESS-S1 might be nudging simulated sea ice to be thicker than the model equilibrium state. We suggest that the thinner sea ice in ACCESS-S2 contributes to the large sea-ice extent variance, but other mechanisms, such as unbalanced initial conditions might also be important.

Given that ACCESS-S2 sea-ice extent is not directly initialised by sea-ice observations, comparing its forecasts with those of ACCESS-S1 allows us to estimate the time-scale over which initial conditions are important. We find that initial conditions affect Antarctic sea-ice forecasts in the order of a few months, but that effect is seasonally dependent. January to April initial conditions improve forecasts for up to three months. February initial conditions in particular are shown to be crucial for determining sea-ice evolution at least up to May. Arctic sea-ice forecasts also show greater sensitivity to initial conditions in boreal summer, compared with boreal winter^{12;47}, suggesting a similar mechanism might be playing a role.

Forecasts initialised in winter have very little skill and ACCESS-S1 and ACCESS-S2 forecast errors are statistically indistinguishable after just two weeks. This is consistent with Libera et al.⁴⁴'s finding of a "winter predictability barrier" in the Weddell Sea, although they describe the barrier as a sharp loss of predictability in July, and here we find a gradual reduction in skill compared with climatology around June. This difference might be due to our use of pan-Antarctic RMSE, since our regional analysis indicates that the degraded skill is most dramatic in the King Haakon Sea.

1335 These findings have important implications for both operational forecasting, model
1336 development and predictability studies. For operational centers, our results suggest that
1337 efforts to improve sea-ice data assimilation should prioritize the summer and autumn
1338 months when initial conditions have the greatest impact on forecast skill. Additionally,
1339 the substantial bias in ACCESS-S2 highlights the need for improved model physics,
1340 particularly in the representation of sea-ice thermodynamics and radiation processes.
1341 Crucially, our results suggest dramatic seasonal variations in sea-ice predictability.
1342 Future studies should therefore use initial conditions through the whole year rather
1343 than focusing on a limited number of initialisation dates.
1344

1350

1351

1352 **Acknowledgments**

1353

1354

1355 We thank the internal reviewers Bethan White and Xiaobing Zhou for their comments
1356 and feedback.

1358

1359 This work benefited from earlier unpublished work by Laura Davies, Phil Reid, Andrew
1360 G. Marshall.

1361

1362

1363 This research was undertaken with the assistance of resources from the National
1364 Computational Infrastructure (NCI Australia), an NCRIS enabled capability supported
1365 by the Australian Government.

1366

1367 This work was supported by ARC SRIEAS Grant SR200100005 Securing Antarctica's
1368 Environmental Future.

1369

1370

1371 **Code and data availability**

1372

1373

1374 The underlying code for this study is available on GitHub and can be accessed via
1375

1376 this link https://github.com/eliocamp/access-s2_ice-eval.

1377

1378

1379

1380

Raw data of ACCESS-S1 and ACCESS-S2 forecasts are not available due to size. 1381
Derived datasets required to reproduce the results are available in this Zenodo 1382
repository: <https://zenodo.org/records/17479538>⁴⁸ 1383

References

- [1] De Silva, L.W.A., Inoue, J., Yamaguchi, H., Terui, T.: Medium range sea ice prediction in support of Japanese research vessel MIRAI's expedition cruise in 2018. *Polar Geography* **43**(2-3), 223–239 (2020) <https://doi.org/10.1080/1088937X.2019.1707317> 1384
1385
1386
1387
1388
1389
1390
1391
1392
1393
1394
1395
1396
1397
1398
1399
1400
1401
1402
1403
1404
1405
1406
1407
1408
1409
1410
1411
1412
1413
1414
1415
1416
1417
1418
1419
1420
1421
1422
1423
1424
1425
1426
- [2] Wagner, P.M., Hughes, N., Bourbonnais, P., Stroeve, J., Rabenstein, L., Bhatt, U., Little, J., Wiggins, H., Fleming, A.: Sea-ice information and forecast needs for industry maritime stakeholders. *Polar Geography* **43**(2-3), 160–187 (2020) <https://doi.org/10.1080/1088937X.2020.1766592>
- [3] Rinke, A., Maslowski, W., Dethloff, K., Clement, J.: Influence of sea ice on the atmosphere: A study with an Arctic atmospheric regional climate model. *Journal of Geophysical Research: Atmospheres* **111**(D16) (2006) <https://doi.org/10.1029/2005JD006957>
- [4] Wang, Z., Fraser, A.D., Reid, P., Coleman, R., O'Farrell, S.: The Influence of Time-Varying Sea Ice Concentration on Antarctic and Southern Ocean Numerical Weather Prediction. *Weather and Forecasting* **39**(2), 293–310 (2024) <https://doi.org/10.1175/WAF-D-22-0220.1>. Chap. *Weather and Forecasting*
- [5] Semmler, T., Kasper, M.A., Jung, T., Serrar, S.: Remote impact of the Antarctic atmosphere on the southern mid?latitudes. *Meteorologische Zeitschrift* **25**(1), 71–77 (2016) <https://doi.org/10.1127/metz/2015/0685>

- 1427 [6] Zampieri, L., Goessling, H.F., Jung, T.: Predictability of Antarctic Sea Ice Edge
1428 on Subseasonal Time Scales. *Geophysical Research Letters* **46**(16), 9719–9727
1429 (2019) <https://doi.org/10.1029/2019GL084096>
- 1430 [7] Gao, Y., Xiu, Y., Nie, Y., Luo, H., Yang, Q., Zampieri, L., Lv, X., Uotila,
1431 P.: An Assessment of Subseasonal Prediction Skill of the Antarctic Sea Ice
1432 Edge. *Journal of Geophysical Research: Oceans* **129**(11), 2024–021499 (2024)
1433 <https://doi.org/10.1029/2024JC021499>
- 1434 [8] Massonnet, F., Barreira, S., Barthélémy, A., Bilbao, R., Blanchard-Wrigglesworth,
1435 E., Blockley, E., Bromwich, D.H., Bushuk, M., Dong, X., Goessling, H.F., Hobbs,
1436 W., Iovino, D., Lee, W.-S., Li, C., Meier, W.N., Merryfield, W.J., Moreno-
1437 Chamarro, E., Morioka, Y., Li, X., Niraula, B., Petty, A., Sanna, A., Scilingo, M.,
1438 Shu, Q., Sigmond, M., Sun, N., Tietsche, S., Wu, X., Yang, Q., Yuan, X.: SIPN
1439 South: Six years of coordinated seasonal Antarctic sea ice predictions. *Frontiers*
1440 in Marine Science **10** (2023) <https://doi.org/10.3389/fmars.2023.1148899>
- 1441 [9] Dong, X., Yang, Q., Nie, Y., Zampieri, L., Wang, J., Liu, J., Chen, D.: Antarctic
1442 sea ice prediction with A convolutional long short-term memory network. *Ocean*
1443 *Modelling* **190**, 102386 (2024) <https://doi.org/10.1016/j.ocemod.2024.102386>
- 1444 [10] Lin, Y., Yang, Q., Li, X., Dong, X., Luo, H., Nie, Y., Wang, J., Wang, Y., Min,
1445 C.: Ice-kNN-South: A Lightweight Machine Learning Model for Antarctic Sea Ice
1446 Prediction. *Journal of Geophysical Research: Machine Learning and Computation*
1447 **2**(1), 2024–000433 (2025) <https://doi.org/10.1029/2024JH000433>
- 1448 [11] Guemas, V., Chevallier, M., Déqué, M., Bellprat, O., Doblas-Reyes, F.: Impact
1449 of sea ice initialization on sea ice and atmosphere prediction skill on seasonal
1450 timescales. *Geophysical Research Letters* **43**(8), 3889–3896 (2016) <https://doi.org/10.1002/2015GL066626>
- 1451
- 1452
- 1453
- 1454
- 1455
- 1456
- 1457
- 1458
- 1459
- 1460
- 1461
- 1462
- 1463
- 1464
- 1465
- 1466
- 1467
- 1468
- 1469
- 1470
- 1471
- 1472

- [12] Day, J.J., Hawkins, E., Tietsche, S.: Will Arctic sea ice thickness initialization improve seasonal forecast skill? *Geophysical Research Letters* **41**(21), 7566–7575 (2014) <https://doi.org/10.1002/2014GL061694> 1473
1474
1475
1476
1477
1478
1479
1480
1481
1482
1483
1484
1485
- [13] Holland, M.M., Blanchard-Wrigglesworth, E., Kay, J., Vavrus, S.: Initial-value predictability of Antarctic sea ice in the Community Climate System Model 3. *Geophysical Research Letters* **40**(10), 2121–2124 (2013) <https://doi.org/10.1002/grl.50410> 1479
1480
1481
1482
1483
1484
1485
- [14] Marchi, S., Fichefet, T., Goosse, H.: Respective influences of perturbed atmospheric and ocean–sea ice initial conditions on the skill of seasonal Antarctic sea ice predictions: A study with NEMO3.6–LIM3. *Ocean Modelling* **148**, 101591 (2020) <https://doi.org/10.1016/j.ocemod.2020.101591> 1486
1487
1488
1489
1490
1491
1492
1493
1494
1495
1496
1497
1498
1499
1500
- [15] Morioka, Y., Iovino, D., Cipollone, A., Masina, S., Behera, S.K.: Decadal Sea Ice Prediction in the West Antarctic Seas with Ocean and Sea Ice Initializations. *Communications Earth & Environment* **3**(1), 189 (2022) <https://doi.org/10.1038/s43247-022-00529-z> 1501
1502
1503
1504
1505
1506
1507
1508
1509
1510
1511
- [16] Wedd, R., Alves, O., Burgh-Day, C., Down, C., Griffiths, M., Hendon, H.H., Hudson, D., Li, S., Lim, E.-P., Marshall, A.G., Shi, L., Smith, P., Smith, G., Spillman, C.M., Wang, G., Wheeler, M.C., Yan, H., Yin, Y., Young, G., Zhao, M., Xiao, Y., Zhou, X.: ACCESS-S2: The upgraded Bureau of Meteorology multi-week to seasonal prediction system. *Journal of Southern Hemisphere Earth Systems Science* **72**(3), 218–242 (2022) <https://doi.org/10.1071/ES22026> 1512
1513
1514
1515
1516
1517
1518
- [17] Hudson, D., Alves, O., Hendon, H.H., Lim, E.-P., Liu, G., Luo, J.-J., MacLachlan, C., Marshall, A.G., Shi, L., Wang, G., Wedd, R., Young, G., Zhao, M., Zhou, X.: ACCESS-S1 The new Bureau of Meteorology multi-week to seasonal prediction system. *Journal of Southern Hemisphere Earth Systems Science* **67**(3), 132–159

- 1519 (2017) <https://doi.org/10.1071/es17009>
1520
1521 [18] Williams, K.D., Harris, C.M., Bodas-Salcedo, A., Camp, J., Comer, R.E., Copsey,
1522 D., Fereday, D., Graham, T., Hill, R., Hinton, T., Hyder, P., Ineson, S., Masato,
1523 G., Milton, S.F., Roberts, M.J., Rowell, D.P., Sanchez, C., Shelly, A., Sinha, B.,
1524 Walters, D.N., West, A., Woollings, T., Xavier, P.K.: The Met Office Global
1525 Coupled model 2.0 (GC2) configuration. *Geoscientific Model Development* **8**(5),
1526 1509–1524 (2015) <https://doi.org/10.5194/gmd-8-1509-2015>
1527
1528
1529
1530
1531
1532 [19] Waters, J., Bell, M.J., Martin, M.J., Lea, D.J.: Reducing ocean model imbalances
1533 in the equatorial region caused by data assimilation. *Quarterly Journal of the Royal*
1534 *Meteorological Society* **143**(702), 195–208 (2017) <https://doi.org/10.1002/qj.2912>
1535
1536
1537
1538 [20] Best, M.J., Pryor, M., Clark, D.B., Rooney, G.G., Essery, R.L.H., Ménard, C.B.,
1539 Edwards, J.M., Hendry, M.A., Porson, A., Gedney, N., Mercado, L.M., Sitch,
1540 S., Blyth, E., Boucher, O., Cox, P.M., Grimmond, C.S.B., Harding, R.J.: The
1541 Joint UK Land Environment Simulator (JULES), model description – Part 1:
1542 Energy and water fluxes. *Geoscientific Model Development* **4**(3), 677–699 (2011)
1543
1544
1545
1546
1547
1548
1549 [21] Gurvan, M., Bourdallé-Badie, R., Bouttier, P.-A., Bricaud, C., Bruciaferri, D.,
1550 Calvert, D., Chanut, J., Clementi, E., Coward, A., Delrosso, D., Ethé, C., Flavoni,
1551 S., Graham, T., Harle, J., Iovino, D., Lea, D., Lévy, C., Lovato, T., Martin,
1552 N., Masson, S., Mocavero, S., Paul, J., Rousset, C., Storkey, D., Storto, A.,
1553 Vancoppenolle, M.: NEMO ocean engine (2013) <https://doi.org/10.5281/zenodo.1475234>
1554
1555
1556
1557
1558
1559
1560 [22] Megann, A., Storkey, D., Aksenov, Y., Alderson, S., Calvert, D., Graham, T.,
1561 Hyder, P., Siddorn, J., Sinha, B.: GO5.0: The joint NERC–Met Office NEMO
1562 global ocean model for use in coupled and forced applications. *Geoscientific Model*
1563
1564

- Development **7**(3), 1069–1092 (2014) <https://doi.org/10.5194/gmd-7-1069-2014> 1565
 1566
- [23] Rae, J.G.L., Hewitt, H.T., Keen, A.B., Ridley, J.K., West, A.E., Harris, C.M., Hunke, E.C., Walters, D.N.: Development of the Global Sea Ice 6.0 CICE configuration for the Met Office Global Coupled model. Geoscientific Model Development **8**(7), 2221–2230 (2015) <https://doi.org/10.5194/gmd-8-2221-2015> 1567
 1568
 1569
 1570
 1571
 1572
 1573
 1574
 1575
 1576
 1577
 1578
 1579
 1580
 1581
 1582
 1583
 1584
 1585
 1586
 1587
 1588
 1589
 1590
 1591
 1592
 1593
 1594
 1595
 1596
 1597
 1598
 1599
 1600
 1601
 1602
 1603
 1604
 1605
 1606
 1607
 1608
 1609
 1610
- [24] Dee, D.P., Uppala, S.M., Simmons, A.J., Berrisford, P., Poli, P., Kobayashi, S., Andrae, U., Balmaseda, M.A., Balsamo, G., Bauer, P., Bechtold, P., Beljaars, A.C.M., van de Berg, L., Bidlot, J., Bormann, N., Delsol, C., Dragani, R., Fuentes, M., Geer, A.J., Haimberger, L., Healy, S.B., Hersbach, H., Hólm, E.V., Isaksen, L., Kållberg, P., Köhler, M., Matricardi, M., McNally, A.P., Monge-Sanz, B.M., Morcrette, J.-J., Park, B.-K., Peubey, C., de Rosnay, P., Tavolato, C., Thépaut, J.-N., Vitart, F.: The ERA-Interim reanalysis: Configuration and performance of the data assimilation system. Quarterly Journal of the Royal Meteorological Society **137**(656), 553–597 (2011) <https://doi.org/10.1002/qj.828>
- [25] Waters, J., Lea, D.J., Martin, M.J., Mirouze, I., Weaver, A., While, J.: Implementing a variational data assimilation system in an operational 1/4 degree global ocean model. Quarterly Journal of the Royal Meteorological Society **141**(687), 333–349 (2015) <https://doi.org/10.1002/qj.2388>
- [26] Good, S.A., Martin, M.J., Rayner, N.A.: EN4: Quality controlled ocean temperature and salinity profiles and monthly objective analyses with uncertainty estimates. Journal of Geophysical Research: Oceans **118**(12), 6704–6716 (2013) <https://doi.org/10.1002/2013JC009067>
- [27] Reynolds, R.W., Smith, T.M., Liu, C., Chelton, D.B., Casey, K.S., Schlax, M.G.: Daily High-Resolution-Blended Analyses for Sea Surface Temperature. Journal of Climate **20**(22), 5473–5496 (2007) <https://doi.org/10.1175/2007JCLI1824.1>.

- 1611 Chap. Journal of Climate
1612
1613 [28] Zweng, M.M., Reagan, J.R., Antonov, J.I., Locarnini, R.A., Mishonov, A.V.,
1614 Boyer, T.P., Garcia, H.E., Baranova, O.K., Johnson, D.R., Seidov, D., Biddle,
1615 M.M.: World ocean atlas 2013. Volume 2, Salinity (2013) <https://doi.org/10.7289/V5251G4D>
1616
1617
1618
1619
1620
1621 [29] Meier, W.N., Stewart, J.S.: Assessing uncertainties in sea ice extent climate
1622 indicators. Environmental Research Letters **14**(3), 035005 (2019) <https://doi.org/10.1088/1748-9326/aaf52c>
1623
1624
1625
1626
1627 [30] Meier, W.N., Peng, G., Scott, D.J., Savoie, M.H.: Verification of a new NOAA/N-
1628 SIDC passive microwave sea-ice concentration climate record. Polar Research
1629
1630 (2014) <https://doi.org/10.3402/polar.v33.21004>
1631
1632
1633 [31] Cavalieri, D.J., Gloersen, P., Campbell, W.J.: Determination of sea ice parameters
1634 with the NIMBUS 7 SMMR. Journal of Geophysical Research: Atmospheres
1635
1636 **89**(D4), 5355–5369 (1984) <https://doi.org/10.1029/JD089iD04p05355>
1637
1638
1639 [32] Comiso, J.: Bootstrap Sea Ice Concentrations from Nimbus-7 SMMR and DMSP
1640 SSM/I-SSMIS. (NSIDC-0079, Version 4). NASA National Snow and Ice Data
1641 Center Distributed Active Archive Center., Boulder, Colorado USA. (2023). <https://doi.org/10.5067/X5LG68MH013O>
1642
1643
1644
1645
1646 [33] Meier, W.N., Fetterer, F., Windnagel, A.K., Stewart, J.S.: NOAA/NSIDC Climate
1647 Data Record of Passive Microwave Sea Ice Concentration. National Snow and Ice
1648 Data Center., Boulder, Colorado USA (2021). <https://doi.org/10.7265/efmz-2t65>
1649
1650
1651
1652 [34] EUMETSAT Ocean and Sea Ice Satellite Application Facility: Global Sea Ice Con-
1653 centration Climate Data Record 1978-2020 (v3.0, 2022), OSI-450-a, <https://cds.climate.copernicus.eu/cdsapp#!/dataset/satellite-sea-ice-concentration>
1654
1655
1656

- [35] Cavalieri, D.J., Crawford, J.P., Drinkwater, M.R., Eppler, D.T., Farmer, L.D., Jentz, R.R., Wackerman, C.C.: Aircraft active and passive microwave validation of sea ice concentration from the Defense Meteorological Satellite Program special sensor microwave imager. *Journal of Geophysical Research: Oceans* **96**(C12), 21989–22008 (1991) <https://doi.org/10.1029/91JC02335>
- [36] Murphy, A.H., Daan, H.: Forecast Evaluation. In: *Probability, Statistics, And Decision Making In The Atmospheric Sciences*. CRC Press, ??? (1985)
- [37] R Core Team: R: A Language and Environment for Statistical Computing. R Foundation for Statistical Computing, Vienna, Austria (2020). R Foundation for Statistical Computing
- [38] Dowle, M., Srinivasan, A.: Data.Table: Extension of 'Data.Frame' (2020)
- [39] Campitelli, E.: metR: Tools for Easier Analysis of Meteorological Fields (2020)
- [40] Schulzweida, U.: CDO User Guide (2023) <https://doi.org/10.5281/ZENODO.100020800>
- [41] Wickham, H.: Ggplot2: Elegant Graphics for Data Analysis. Use R! Springer, New York (2009). <https://doi.org/10.1007/978-0-387-98141-3>
- [42] Xie, Y.: Dynamic Documents with R and Knitr, 2nd edn. Chapman and Hall/CRC, Boca Raton, Florida (2015)
- [43] Allaire, J.J., Teague, C., Xie, Y., Dervieux, C.: Quarto. Zenodo (2022). <https://doi.org/10.5281/ZENODO.5960048>
- [44] Libera, S., Hobbs, W., Klocker, A., Meyer, A., Matear, R.: Ocean-Sea Ice Processes and Their Role in Multi-Month Predictability of Antarctic Sea Ice. *Geophysical Research Letters* **49**(8), 2021–097047 (2022) <https://doi.org/10.1029/>

1703 2021GL097047
1704
1705 [45] Roach, L.A., Dörr, J., Holmes, C.R., Massonnet, F., Blockley, E.W., Notz, D.,
1706 Rackow, T., Raphael, M.N., O'Farrell, S.P., Bailey, D.A., Bitz, C.M.: Antarctic
1707 Sea Ice Area in CMIP6. Geophysical Research Letters **47**(9), 2019–086729 (2020)
1708
1709 <https://doi.org/10.1029/2019GL086729>
1710
1711
1712
1713 [46] Zhou, X., Alves, O.: Evaluating sea ice in ACCESS-S2. Technical report, Bureau
1714 of Meteorology (2022)
1715
1716
1717 [47] Bunzel, F., Notz, D., Baehr, J., Müller, W.A., Fröhlich, K.: Seasonal climate
1718 forecasts significantly affected by observational uncertainty of Arctic sea ice
1719 concentration. Geophysical Research Letters **43**(2), 852–859 (2016) <https://doi.org/10.1002/2015GL066928>
1720
1721
1722
1723
1724
1725 [48] Campitelli, E.: Data for "Evaluating the Importance of Initial Conditions for
1726 Antarctic Sea Ice Seasonal Predictability with a Fully Coupled Forecast Model".
1727
1728 Zenodo (2025). <https://doi.org/10.5281/ZENODO.17479537>
1729
1730
1731
1732
1733
1734
1735
1736
1737
1738
1739
1740
1741
1742
1743
1744
1745
1746
1747
1748

Supplementary figures

The following are the same figures from the main paper but using the OSI dataset instead of CDR.

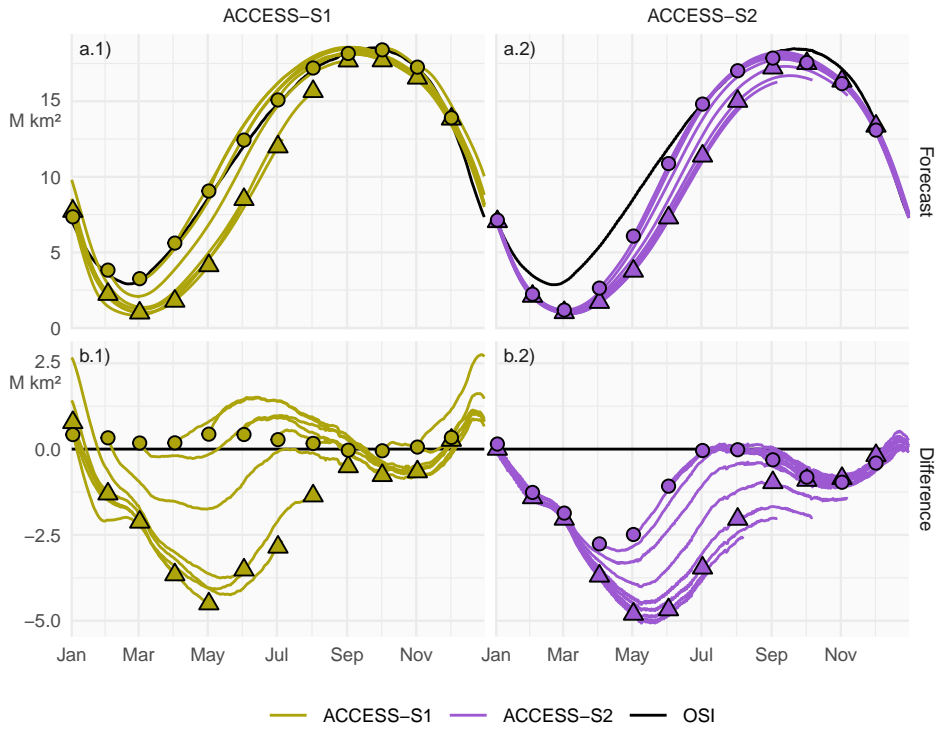
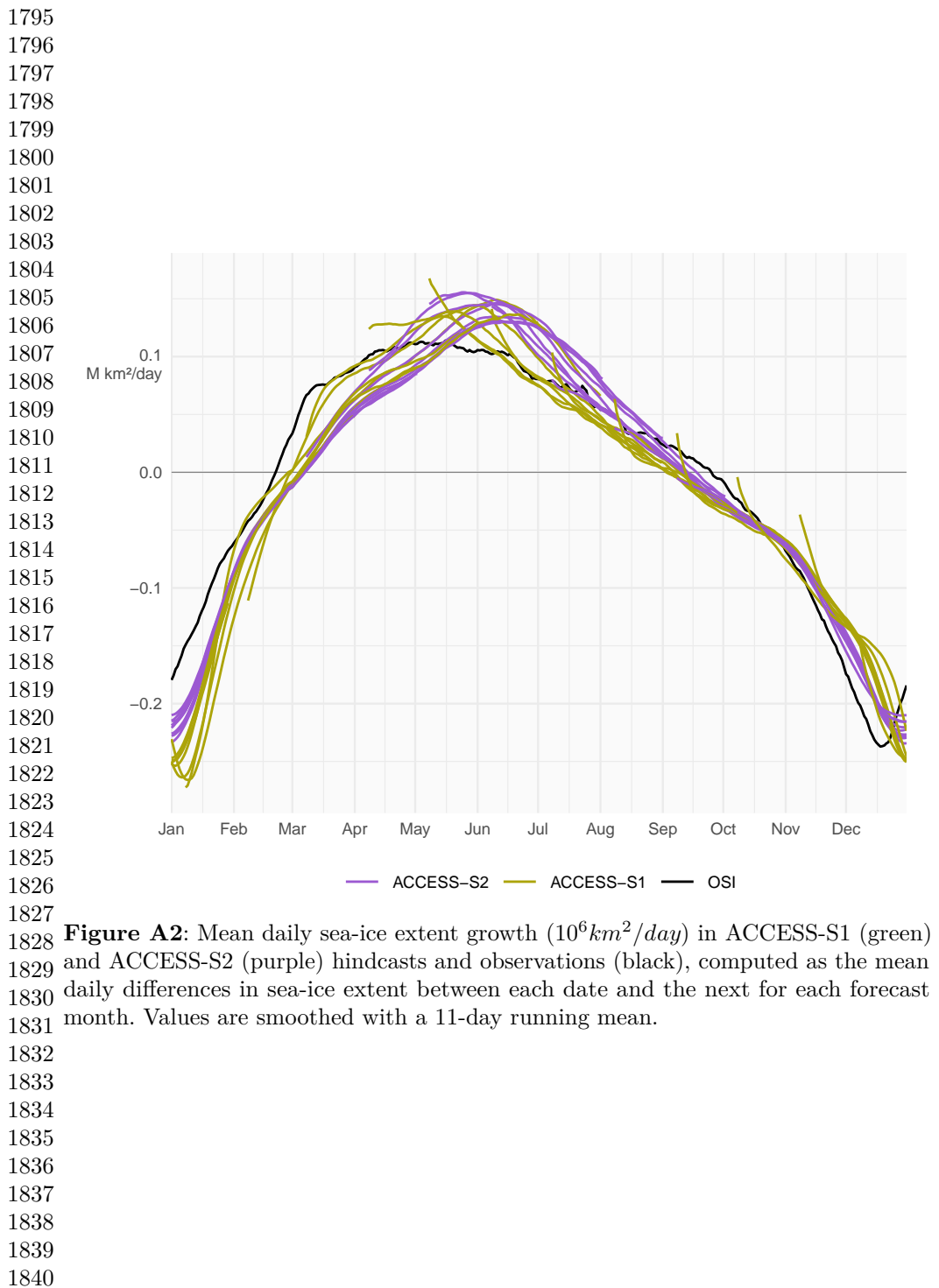


Figure A1: Row a: Pan-Antarctic daily mean sea-ice extent for all hindcasts initialised on the first of each calendar month for ACCESS-S1 (column 1; green) and ACCESS-S2 (column 2; purple). Observed mean sea-ice extent in each corresponding hindcast period is shown in black. Row b: Mean differences between the forecast and the observed values. Circles represent the initial conditions at the start of forecasts (i.e., the first of every month), and triangles represent the mean values at the lead time corresponding to the maximum lead time in S1 (between 213 and 216 days, depending on the month)



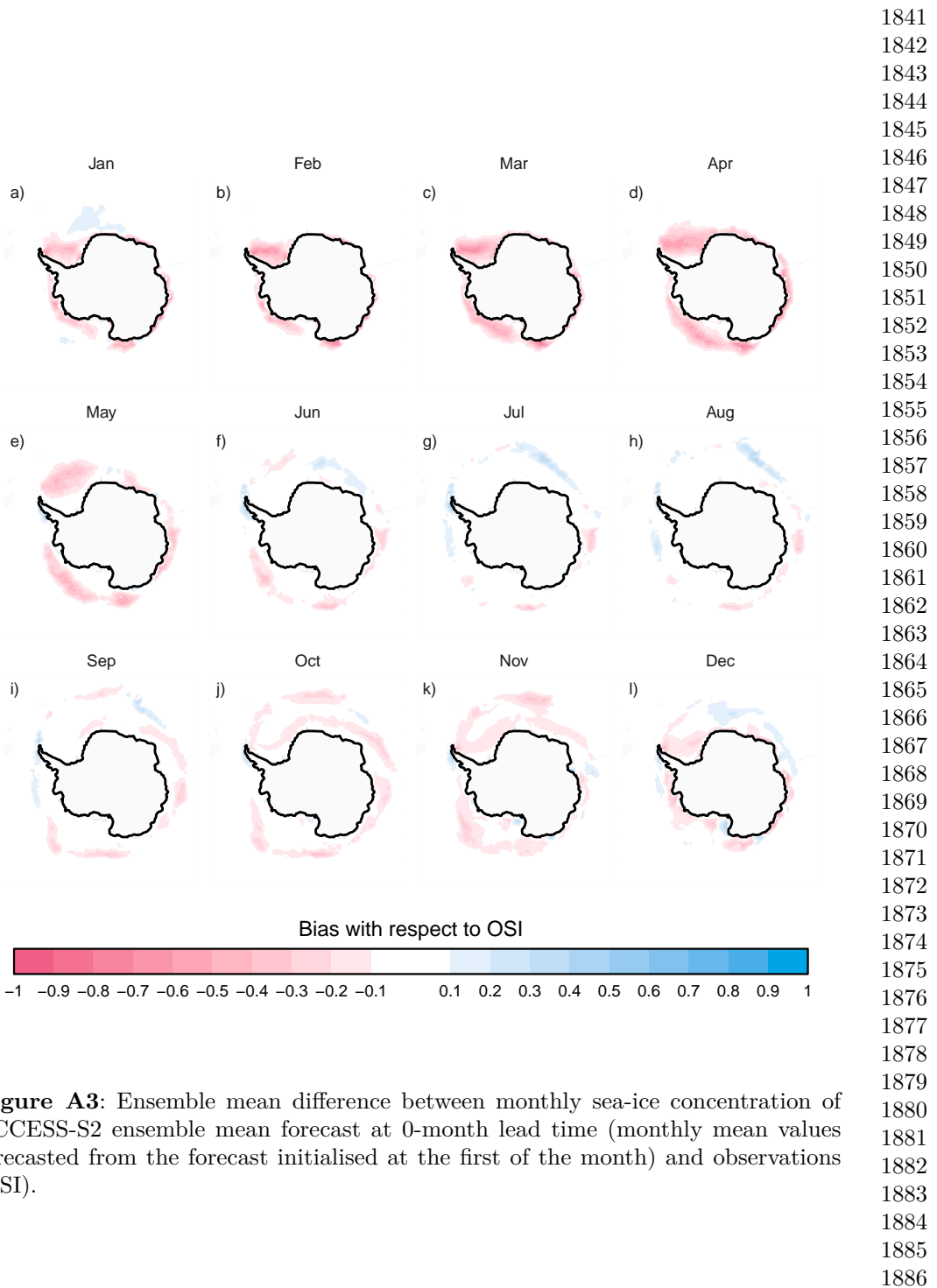
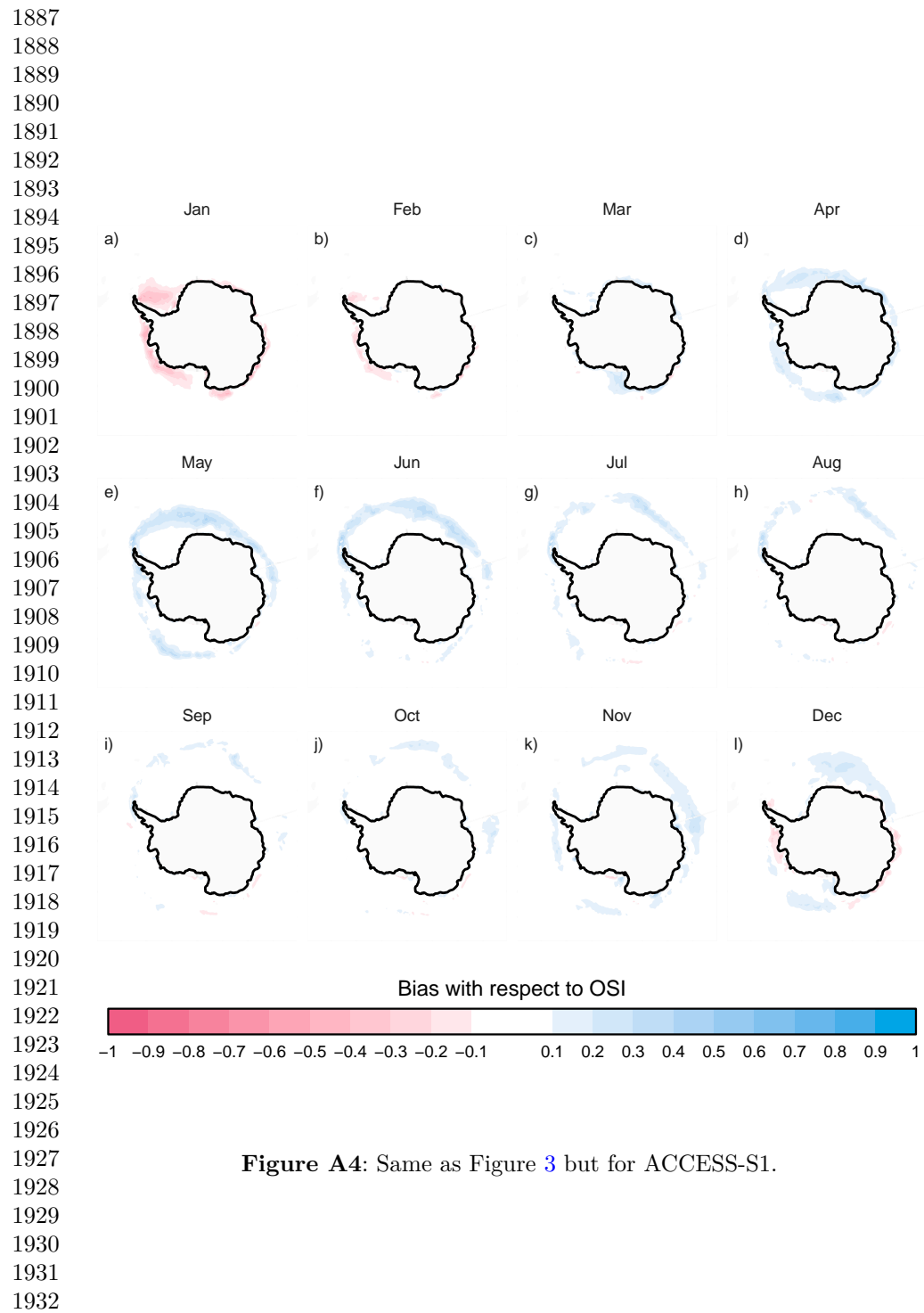


Figure A3: Ensemble mean difference between monthly sea-ice concentration of ACCESS-S2 ensemble mean forecast at 0-month lead time (monthly mean values forecasted from the forecast initialised at the first of the month) and observations (OSI).



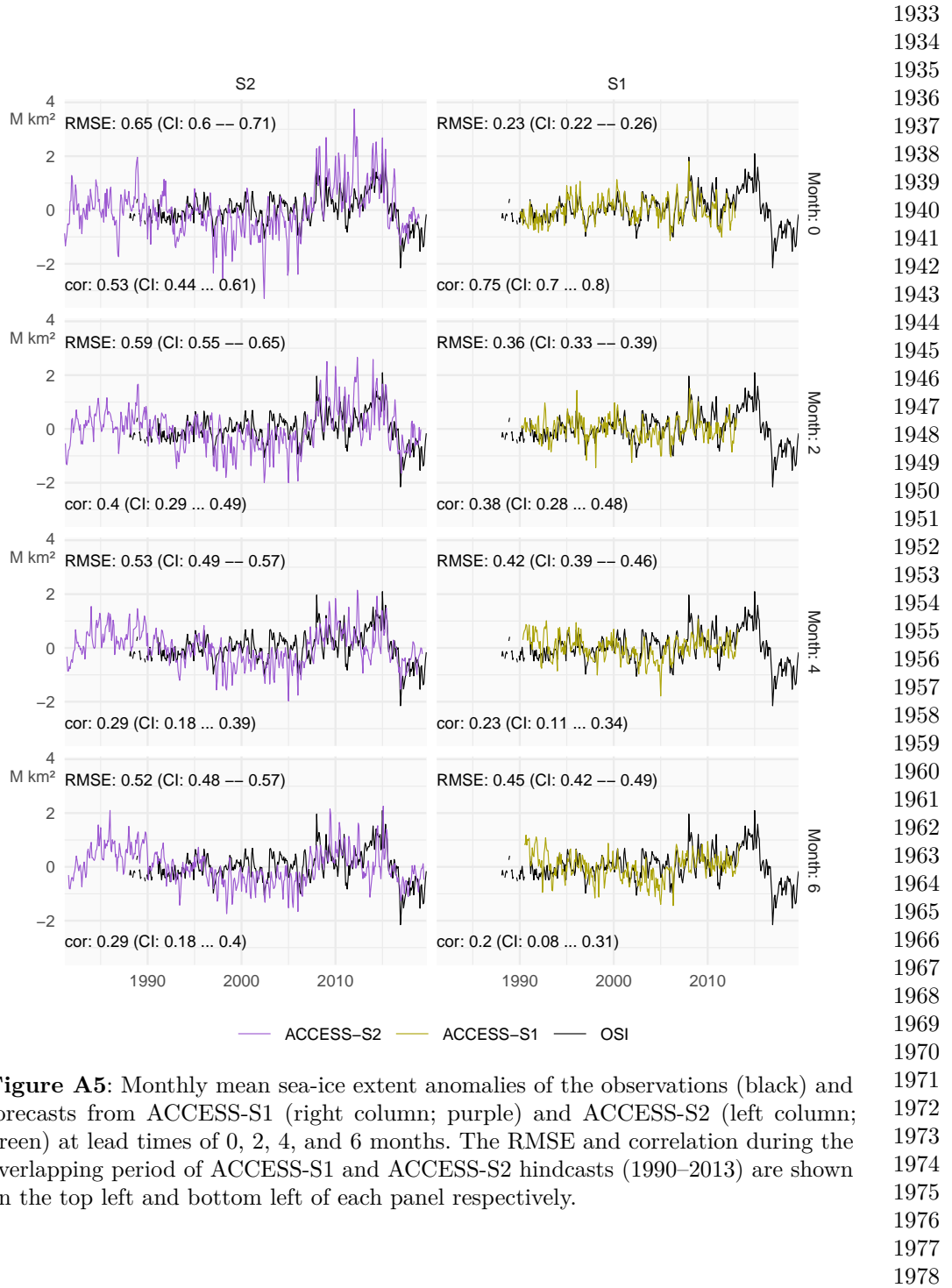


Figure A5: Monthly mean sea-ice extent anomalies of the observations (black) and forecasts from ACCESS-S1 (right column; purple) and ACCESS-S2 (left column; green) at lead times of 0, 2, 4, and 6 months. The RMSE and correlation during the overlapping period of ACCESS-S1 and ACCESS-S2 hindcasts (1990–2013) are shown on the top left and bottom left of each panel respectively.

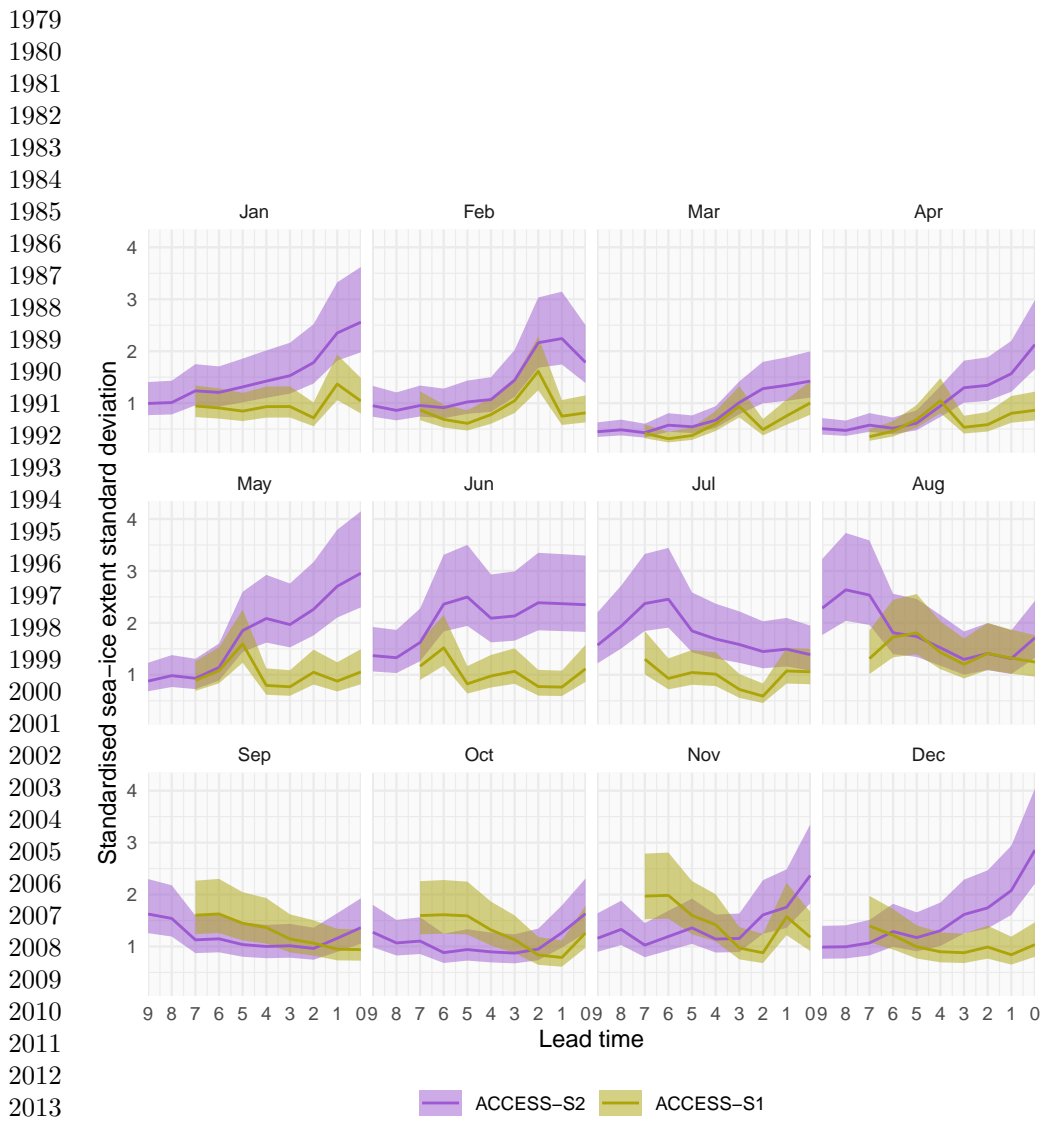


Figure A6: Interannual standard deviation with 95% confidence interval of monthly mean sea-ice extent forecasted for each month divided by that month's sea-ice extent observation standard deviation. ACCESS-S1 and ACCESS-S2 at different lead times. Each panel indicates the target month. Note the reverse horizontal axis.

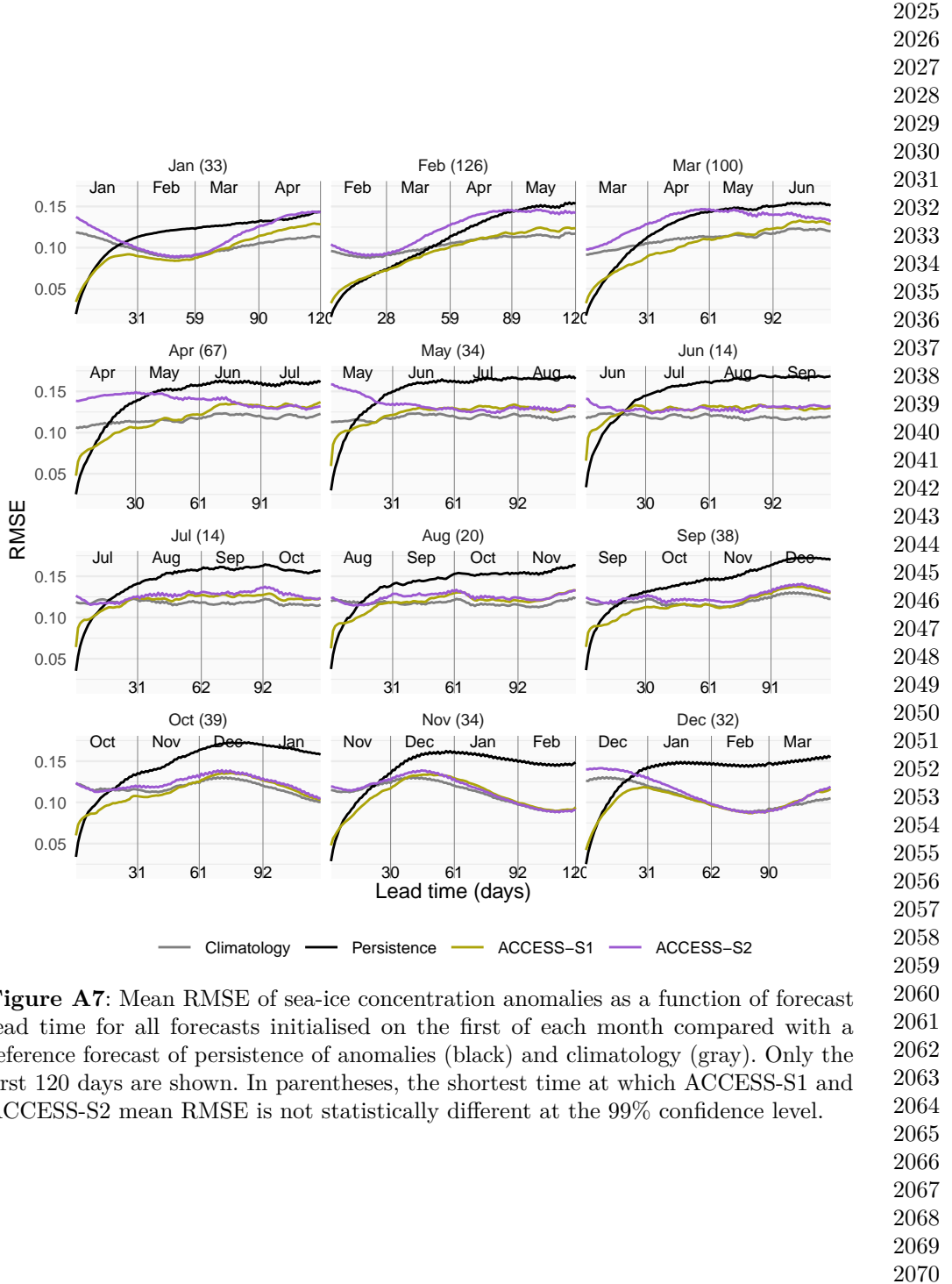
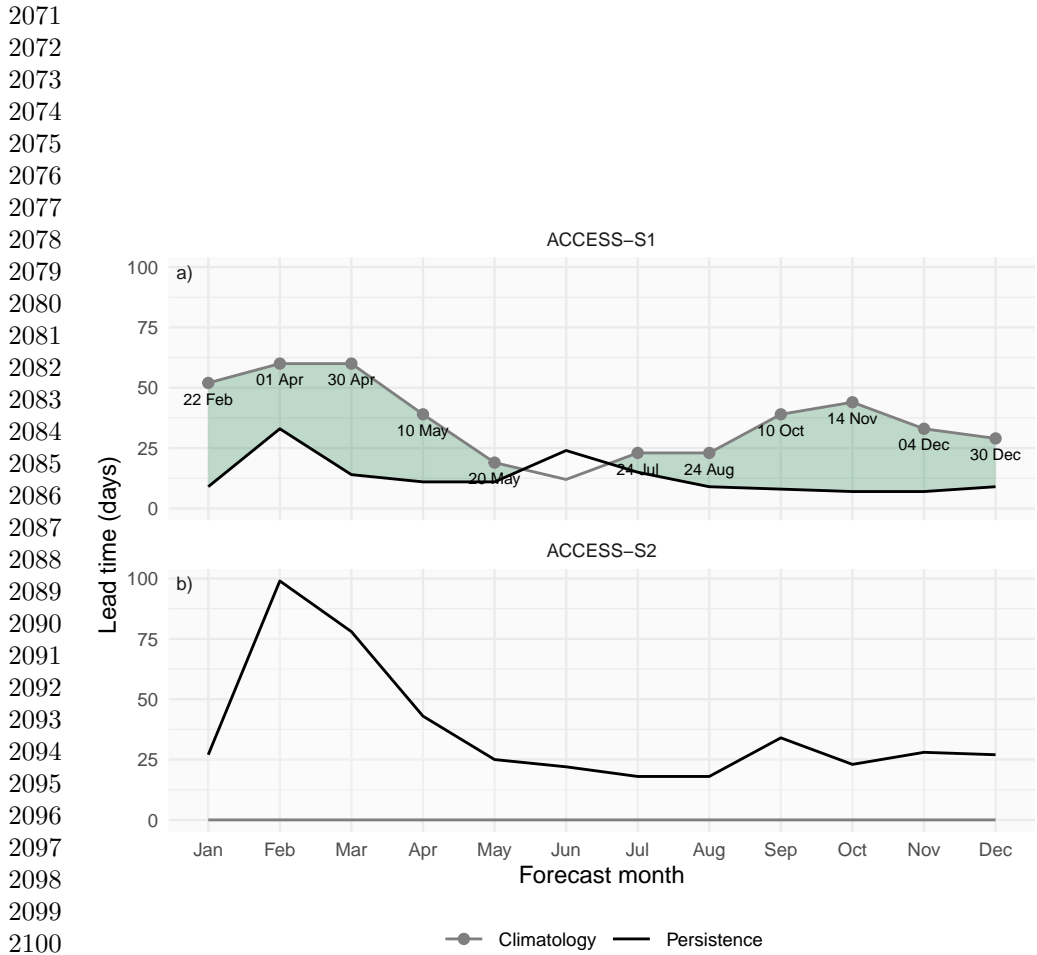


Figure A7: Mean RMSE of sea-ice concentration anomalies as a function of forecast lead time for all forecasts initialised on the first of each month compared with a reference forecast of persistence of anomalies (black) and climatology (gray). Only the first 120 days are shown. In parentheses, the shortest time at which ACCESS-S1 and ACCESS-S2 mean RMSE is not statistically different at the 99% confidence level.



2101 **Figure A8:** Minimum lead time at which each forecast's mean RMSE becomes larger
 2102 than the lower bound of the 95% confidence interval of persistence forecast RMSE
 2103 (black lines) and maximum lead time at which each forecast's mean RMSE remains
 2104 lower than the lower bound of the 95% confidence interval of climatological forecast
 2105 RMSE (gray lines). Green shading indicates the window where forecasts outperform
 2106 both persistence (lead times longer than black line) and climatology (lead times
 2107 shorter than gray line). Text labels show the date corresponding to the maximum lead time at
 2108 which each forecast outperforms climatology.
 2109

2110
 2111
 2112
 2113
 2114
 2115
 2116

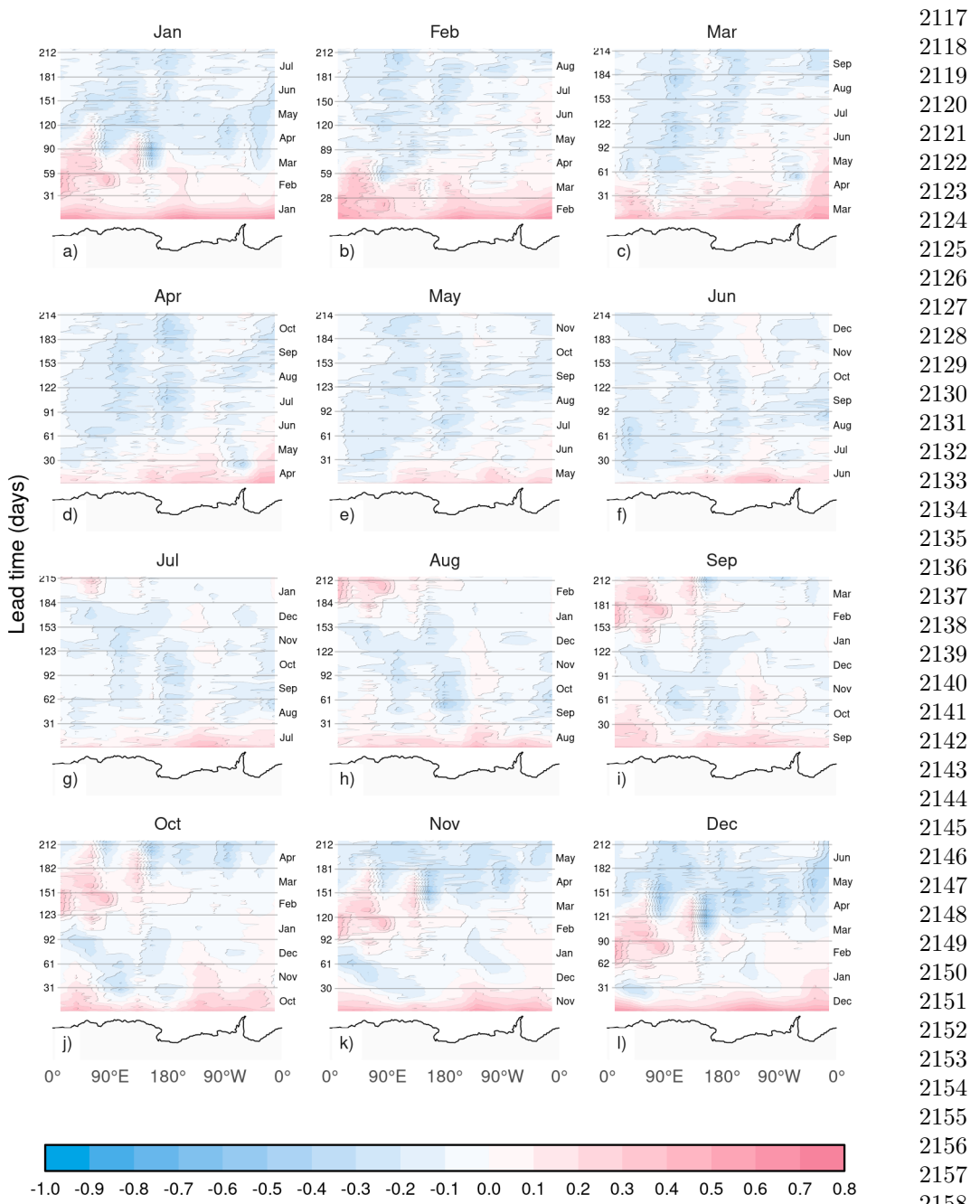


Figure A9: RMSE skill score of ACCESS-S1 forecasts with climatological forecast as reference computed on 15 meridional slices 24° wide as a function of lead time and longitude. Antarctica's coastline is shown at the bottom of each panel for reference.

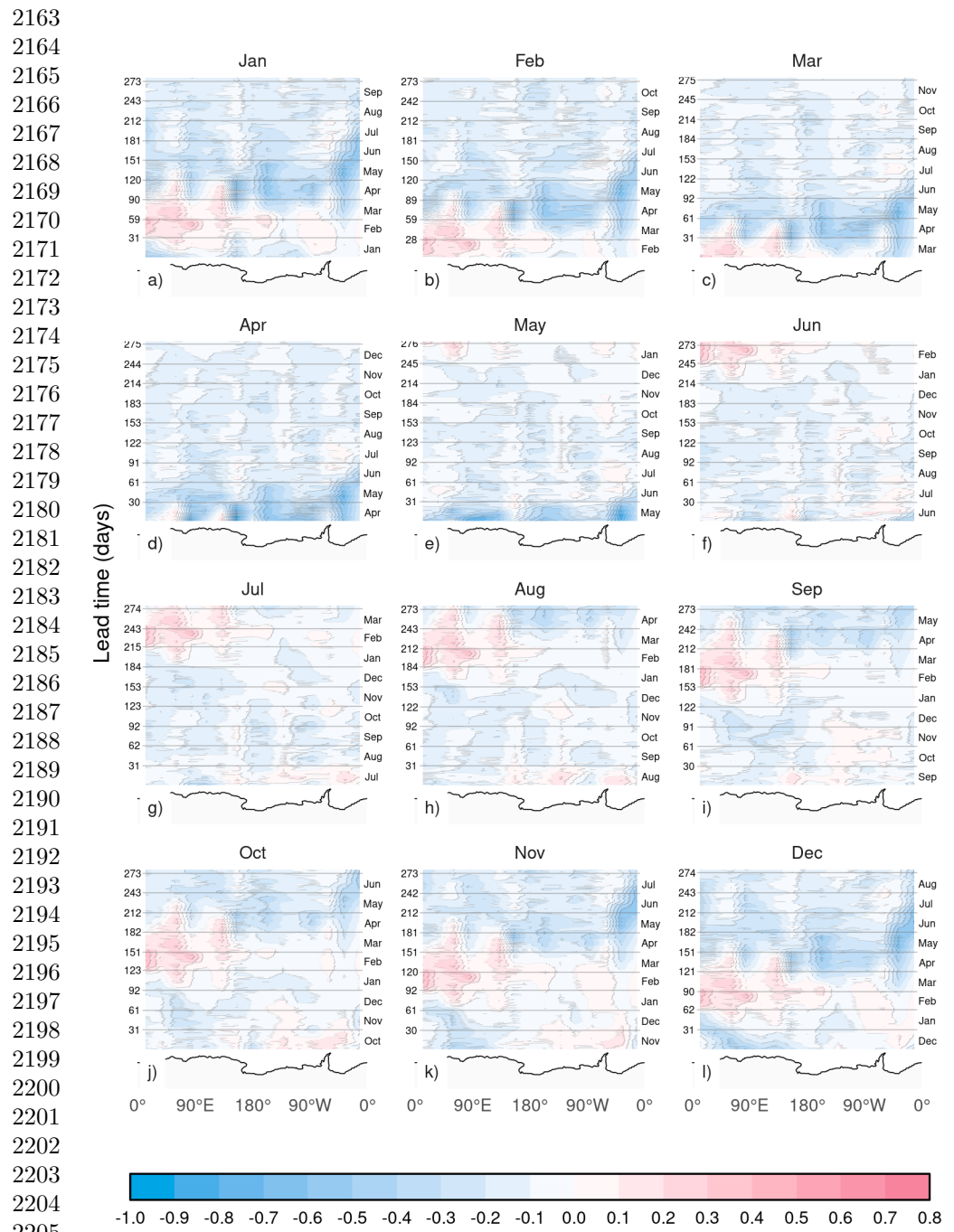


Figure A10: Same as Figure 11 but for ACCESS-S2.

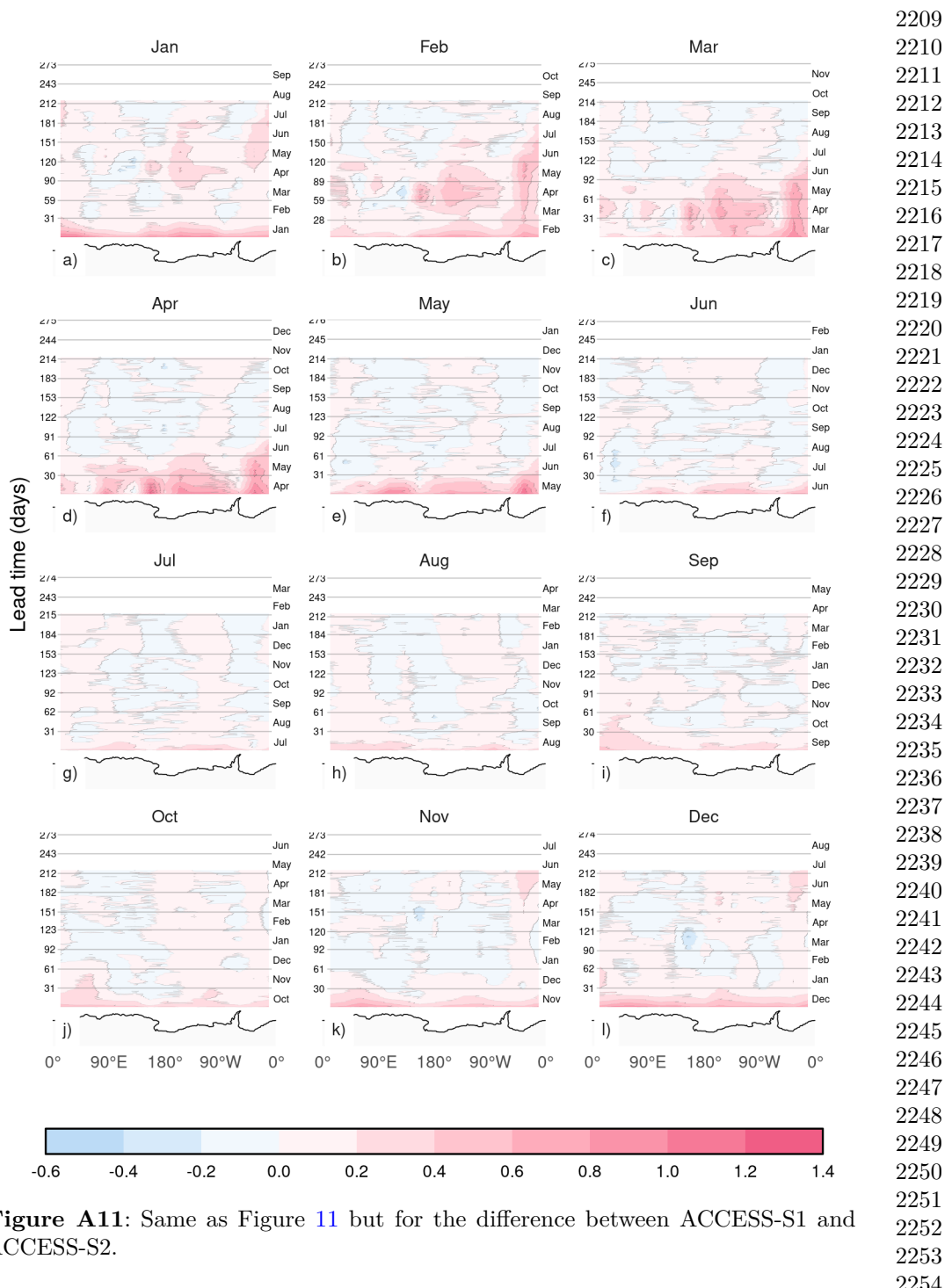
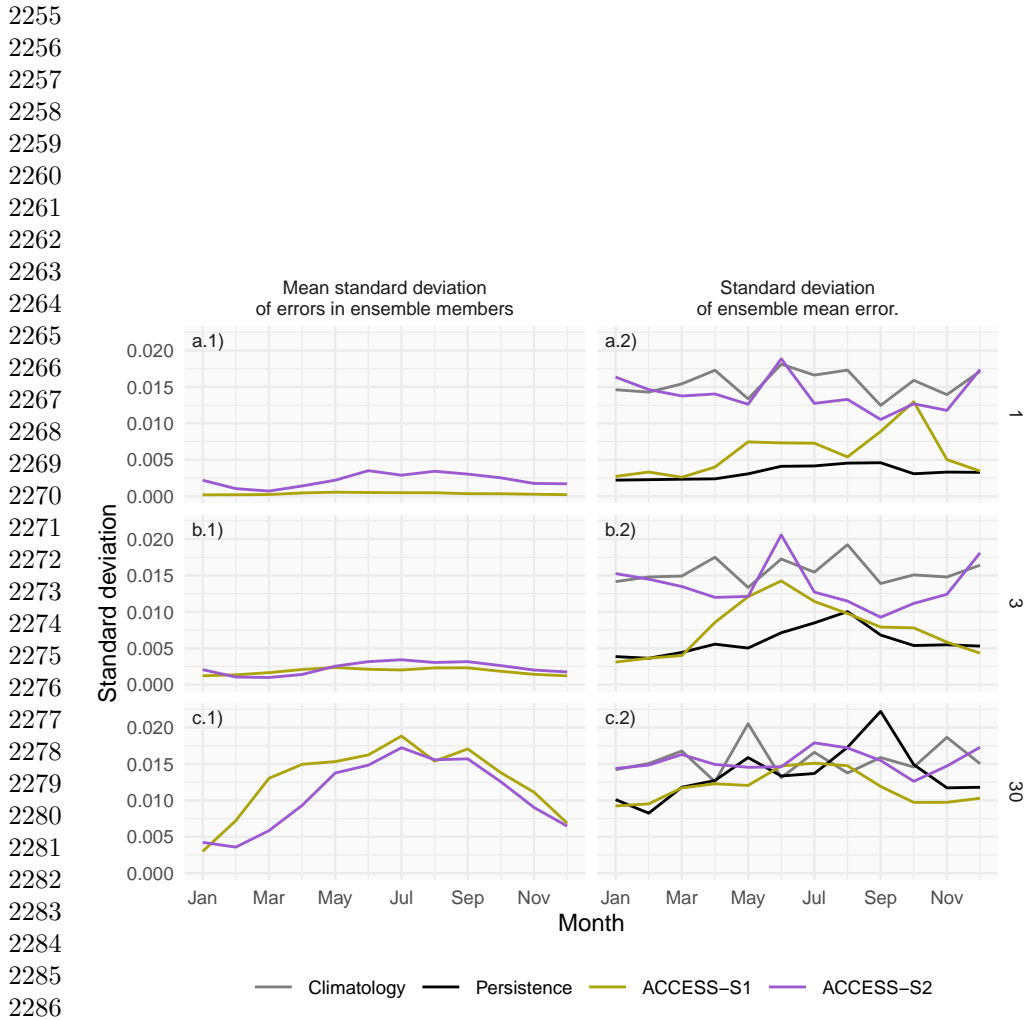


Figure A11: Same as Figure 11 but for the difference between ACCESS-S1 and ACCESS-S2.



2287 **Figure A12:** Decomposition of forecast error spread at 1, 5 and 30 days lead time for
 2288 ACCESS-S1 and ACCESS-S2 hindcasts across initialization months. The left column
 2289 shows the mean standard deviation of RMSE errors across ensemble members, while
 2290 the right column shows the standard deviation of the ensemble mean RMSE error and
 2291 the spread of the persistence and climatology forecasts errors.
 2292
 2293
 2294
 2295
 2296
 2297
 2298
 2299
 2300